Guillermic, M., Lalonde, S., Hendry, K., & Rouxel, O. (2017). The isotope composition of inorganic Germanium in seawater and deep sea sponges. *Geochimica et Cosmochimica Acta*, *212*, 99-118. https://doi.org/10.1016/j.gca.2017.06.011

The isotope composition of inorganic Germanium in seawater and deep sea sponges

Maxence Guillermic[1], Stefan V. Lalonde[1], Katharine R. Hendry[2], Olivier J. Rouxel[3,4*]

[1] Institut Universitaire Européen de la Mer, Laboratoire Domaines Océaniques UMR 6538, Université de Brest, BP 80 F- 29280 Plouzané, France

[2] School of Earth Science, University of Bristol, Wills Memorial Building, Queen's Road, Bristol BS8 IRJ, UK

[3] IFREMER, Centre de Brest, Unité Géosciences Marines, 29280 Plouzané, France

[4] University of Hawaii, Department of Oceanography, Honolulu, HI 96822, USA

Submitted to *Geochimica et Cosmochimica Acta*

*Corresponding author:

E-mail address: orouxel@hawaii.edu

Abstract

Although dissolved concentrations of germanium (Ge) and silicon (Si) in modern seawater are tightly correlated, uncertainties still exist in the modern marine Ge cycle. Germanium stable isotope systematics in marine systems should provide additional constraints on marine Ge sources and sinks, however the low concentration of Ge in seawater presents an analytical challenge for isotopic measurement. Here, we present a new method of pre-concentration of inorganic Ge from seawater which was applied to measure three Ge isotope profiles in the Southern Ocean and deep seawater from the Atlantic and Pacific Oceans. Germanium isotopic measurements were performed on Ge amounts as low as 2.6 ng using a double-spike approach and a hydride generation system coupled to a MC-ICP-MS. Germanium was co-precipitated with iron hydroxide and then purified through anion-exchange chromatography. Results for the deep (i.e. > 1000 m depth) Pacific Ocean off Hawaii (nearby Loihi Seamount) and the deep Atlantic off Bermuda (BATS station) showed nearly identical $\delta^{74/70}$Ge values at 3.19 ± 0.31 ‰ (2SD, n = 9) and 2.93 ± 0.10 ‰ (2SD, n = 2), respectively. Vertical distributions of Ge concentration and isotope composition in the deep Southern Ocean for water depth > 1300 m yielded an average $\delta^{74/70}$Ge = 3.13 ± 0.25 ‰ (2SD, n = 14) and Ge/Si = 0.80 ± 0.09 μmol/mol (2SD, n = 12). Significant variations in $\delta^{74/70}$Ge, from 2.62 to 3.71 ‰, were measured in the first 1000 m in one station of the Southern Ocean near Sars Seamount in the Drake Passage, with the heaviest values measured in surface waters. Isotope fractionation by diatoms during opal biomineralization may explain the enrichment in heavy isotopes for both Ge and Si in surface seawater. However, examination of both oceanographic parameters and $\delta^{74/70}$Ge values suggest also that water mass mixing and potential contribution of shelf-derived Ge also could contribute to the variations. Combining these results with new Ge isotope data for deep-sea sponges sampled nearby allowed us to determine a Ge isotope fractionation factor of -0.87 ± 0.37 ‰ (2SD, n = 12) during Ge uptake by sponges. Although Ge has long been considered as a geochemical twin of Si, this work underpins fundamental differences in their isotopic behaviors both during biomineralization processes and in their oceanic distributions. This suggests that combined with Si isotopes, Ge isotopes hold significant promise as a complementary proxy for delineating biological versus source effects in the evolution of the marine silicon cycle through time.

Keywords: stable isotopes, germanium, silicon, sponges, Southern Ocean, chemical oceanography

1. Introduction

Germanium (Ge) has long been considered a pseudo-heavy isotope of silicon (Si) because it displays similar behavior in marine and terrestrial environments (Froelich and Andreae, 1981). Dissolved inorganic Ge concentrations in seawater range from 0 to about 200 pM and display a correlation with dissolved silica that is remarkably consistent across the world's oceans, underlying its potential as a complementary tracer for marine silicon cycling (Froelich and Andreae, 1981; Froelich et al., 1985a; Froelich et al., 1985b; Ellwood and Maher, 2003). Relatively constant Ge/Si ratios of 0.76 µmol/mol in seawater worldwide suggest that Ge/Si is not fractionated during biological uptake (Murnane and Stallard, 1988; Froelich et al., 1989), although a preferential uptake of Si versus Ge has been observed at low Si concentrations (< 6 µM) (Ellwood and Maher, 2003).

It has been generally thought that oceanic Ge/Si ratios reflect primarily the Ge/Si ratios of the different sources and sinks of Ge and Si in seawater. Seafloor hydrothermal vent fluids at mid-ocean ridges, ridge flanks and volcanic seamounts have Ge/Si ratios of 8 to 14 µmol/mol (Mortlock and Froelich, 1987; Wheat and McManus, 2008; Escoube et al., 2015) whereas Ge/Si ratios in rivers are about 0.54 µmol/mol, with significant temporal and spatial variations (0.1 to 2.5 µmol/mol) that depend on weathering regimes (Mortlock and Froelich, 1987; Kurtz et al., 2011). Ge/Si in rivers is depressed relative to bulk continental crust (Ge/Si = 1.3 µmol/mol) due to the affinity of Ge for iron oxyhydroxides, organic compounds and secondary soil silicates (Kurtz et al., 2002). The elevated Ge/Si ratio of seafloor hydrothermal fluids is likely the result of mineral-fluid partitioning in the reaction zone and the subsurface precipitation of silicate minerals that fractionate against Ge (Mortlock et al., 1993; Pokrovski and Schott, 1998; Escoube et al., 2015). While the major sink of Si in seawater is the burial of biogenic opal in sediments, mass balance of Ge in seawater requires the existence of a non-opal sink, probably associated with an Fe-rich authigenic sink (Hammond et al., 2000; King et al., 2000; McManus et al., 2003; Baronas et al., 2016).

Capitalizing on the promise of the Ge/Si proxy, several studies have explored the use of Ge isotope ratios [defined as $\delta^{74/70}Ge = 1000*(^{74}Ge/^{70}Ge_{sample} / {}^{74}Ge/^{70}Ge_{NIST3120a} - 1)$ as a new geochemical tracer of Ge sources and behavior in oceanic environments and hydrothermal systems (Rouxel et al., 2006; Siebert et al., 2006; Qi et al., 2011; Siebert et al., 2011; Escoube et al., 2012; Belissont et al., 2014; Escoube et al., 2015). Based on the Ge isotope composition of modern marine biogenic opal (e.g. sponges and diatoms), previous

studies have suggested that the Ge isotopic composition of seawater is enriched in heavy isotopes relative to the oceanic crust by up to 2.5 ‰ (Mantoura, 2006; Rouxel et al., 2006). This indirect estimation of the Ge isotope composition of seawater has been used to establish a preliminary isotopic mass balance for Ge in seawater (Escoube et al., 2015). However, due to analytical challenges, the Ge isotopic composition of seawater – and the driving mechanisms behind isotopic fractionation in the marine system – remain unknown. Considering the wealth of previous studies investigating the variations of Si isotopes in seawater (Reynolds et al., 2006; Grasse et al., 2013; de Souza et al., 2014; Cao et al., 2015), the study of Ge isotope systematics in seawater has strong potential both in terms of assessing the global budget of Ge in seawater and also as an oceanographic proxy that could be used in conjunction with Si isotopes to better understand changes in silicon cycling.

Here, we report a method for the pre-concentration and Ge isotope analysis of dissolved inorganic Ge in seawater using online hydride-generation coupled to multi-collector inductively coupled plasma mass spectrometry (MC-ICP-MS). This method is adapted from techniques described previously (Rouxel et al., 2006; Siebert et al., 2006; Siebert et al., 2011; Escoube et al., 2012) and involves: (1) the addition of Ge double-spike (^{73}Ge, ^{70}Ge) to correct for both instrumental mass bias and Ge isotope fractionation during sample preparation; (2) pre-concentration of inorganic Ge by co-precipitation with iron hydroxide ($Fe(OH)_3$), (3) recovery and dissolution of $Fe(OH)_3$ followed by anion-exchange chromatographic purification of Ge, (4) gaseous hydride introduction into the plasma torch allowing for high sensitivity and aqueous matrix-free isotope analysis. We applied this method to obtain the first Ge isotope profiles in seawater using a set of samples from the Southern Ocean that were previously investigated for Si isotopes (Hendry et al., 2010). We also report new measurements of deep seawater from the Atlantic and Pacific Oceans. By comparing $\delta^{74/70}$Ge from sponges and co-located seawater, we also determined the potential influence of biological uptake on fractionation of Ge isotopes and Ge/Si.

2. Materials and methods

2.1. Sample collection

Seawater samples and sponges from the Southern Ocean were collected in May 2011 from the Drake Passage (Southern Ocean) aboard the *R/V Nathaniel B. Palmer*. Seawater

samples were obtained at three stations; "Sars" (59.753°S, 69.057°W; bottom depth at 3141 m) nearby the Sars seamount, "Burdwood Bank" (55.054°S, 62.100°W; bottom depth at 4191 m), and West Antarctic Peninsula (WAP) off Slope (62.067°S, 62.583°W; bottom depth at 4726 m) (Fig. 1). Sampling depths ranged from 2.8 to 3100 m for "Sars", 501 to 4110 m for "Burdwood Bank" and 4.7 to 4718 m for "WAP". Hence, surface seawater was sampled only at two stations. The samples were collected in Niskin bottles during the deep water CTD casts, filtered through 0.4 μm Supor membranes (Pall acropak filters) and stored in pre-cleaned 4 L HDPE bottles. The seawater samples were acidified immediately with hydrochloric acid (Optima grade) to reach a final concentration of 0.1 % v/v and stored until further processing in April 2015. Inorganic $Si(OH)_4$ (referred to as Si in this paper) concentration analyses of seawater were carried out at Woods Hole Oceanographic Institution and have been previously reported in Hendry et al. (2010).

Sponge samples were obtained from living specimens previously investigated for their Si and Zn isotope signatures (Hendry et al., 2010; Hendry and Andersen, 2013). We selected samples from a north-south transect across the Scotia Sea and Drake Passage, with additional samples from the Scotia Sea, encompassing a range of bottom-water Si concentrations (12 to 120 μM) and depths (320 to 2266 m). Sponges were collected aboard the *R/V Nathaniel B. Palmer* (April-May 2008) by either benthic trawl or dredge, and were subsequently stored dried or frozen.

Surface and deep seawater samples from the North Atlantic were obtained from the GEOTRACES IC1 BATS Atlantic intercalibration station (31.667°N; 64.167°W) (Boyle et al., 2012). Although Ge is not considered strictly as contamination-prone element, we selected these samples for documenting potential analytical bias using regular Niskins bottles versus GEOTRACES-compliant rosettes. This set of samples also allows future interlaboratory comparison of seawater Ge isotope values. The GEOTRACES Surface Isotope (GSI) sample was obtained from a 4 L split of a ~500 L tank filled with near surface (7 m) water pumped from the UCSC towed fish. The GEOTRACES Deep Isotope (GDI) sample was obtained from a 4 L split of a ~250 L tank filled from all 24 GO-Flo bottles on the US GEOTRACES trace metal rosette at 2000 m. All samples were filtered on-board at 0.2 μm using Pall Acropak capsule filters and stored acidified at pH 1.8 with purified 6 M HCl.

Deep seawater from the Pacific Ocean was obtained from 3 stations: FeMO Deep (18.700°N;, 155.183°W), Shinkai Deep (18.767°N, 155.117°W) and South West Loihi

(18.867°N, 155.300°W). Samples from FeMO Deep were recovered during the cruise FeMO 2009 (*R/V Kilo Moana*) in October 2009, southeast of the Loihi Seamount (Edwards et al., 2011). Samples from Shinkai Deep and SW Loihi were recovered during the cruise Loihi 2014 (*R/V Falkor*) in July 2014 at the base and around the summit of the Loihi Seamount, respectively. All seawater samples were collected by CTD rosette using 12 L Niskin bottles internally sprung with silicone. Although Loihi Seamount is known for having significant hydrothermal activity at its summit with westward dispersal of a hydrothermal plume containing high concentrations of Fe (Bennett et al., 2011) and potentially Ge (Escoube et al., 2015), we selected samples from areas and water-depths that were removed from the hydrothermal plume (i.e. absence of Fe and Mn anomalies). Because the typical sample size was limited to 1 L, we pooled several samples from a similar range of water depths to obtain sample sizes of 3.5 to 4 L. Hence, for these samples, only the depth range is reported. We analyzed both filtered (through 0.2 µm Supor filters) and unfiltered samples that were acidified to pH 1.8 with 6M HCl (optima grade; Fisher Chemical) prior to analysis.

Large volumes of coastal surface seawater were used for the initial stages of analytical development related to Ge pre-concentration and isotope analysis. This internal standard was obtained from the Bay of Brest in March 2015. It was filtered to 0.45 µm and acidified to pH 2 using concentrated single distilled hydrochloric acid.

2.2. Reagents and germanium standard solutions

The NIST SRM 3120a elemental standard solution (Lot #000411, 10 mg/g) is used in this study as a Ge reference standard, and has been calibrated against other internal standards used in previous Ge isotope studies (Escoube et al., 2012). We used the same double-spike previously employed by Escoube et al. (2012; 2015), prepared from Ge metal spikes ^{73}Ge and ^{70}Ge purchased from Isoflex USA (Ge-70 #32-01-70-3259 and Ge-73 #32-01-73-1405). Each spike was dissolved separately and we obtained the following composition for the double-spike: $^{74}Ge/^{70}Ge = 0.07614 \pm 0.00010$; $^{73}Ge/^{70}Ge = 0.60707 \pm 0.00008$; $^{72}Ge/^{70}Ge = 0.05626 \pm 0.00008$ (2sd uncertainties).

Iron(III) solution used for Ge co-precipitation was prepared by dissolution of $FeCl_3 \cdot 6H_2O$ salt (Acros Organics) in 6 M HCl (single distilled HCl). In order to decrease reagent blanks, the solution was evaporated at 120°C to remove Ge impurities by the

formation of volatile $GeCl_4$ species (Kaya and Volkan, 2011; Luais, 2012). The stock Fe(III) solution was adjusted to a Fe concentration of 12,000 ppm in 3 M HCl.

The hydride generation reagent was made of 10 g of sodium borohydride powder (high purity $NaBH_4$; Fisher Chemical) and 5 g of sodium hydroxide pellets (analytical grade; Acros Organics) dissolved in 1 L of ultrapure water (Milli-Q 18.2 MΩ·cm) and was prepared freshly before each analytical session. During chemical dissolution and purification, high purity HNO_3 (distilled grade) and HF (optima grade; Fisher Chemical) were used.

2.3. Preconcentration of inorganic Ge from seawater

The double-spike (^{70}Ge and ^{73}Ge) was first added to the sample bottle to a spike/natural weight ratio, referred hereafter as s/n, of about 1.0. Although Escoube et al. (2012) showed that Ge isotope measurements are still acceptable with a s/n ratio ranging from 0.4 to 8, we found that a narrower s/n ratio of 0.7 to 1.3 provided optimal analytical conditions. Hence, this method requires the prior knowledge of Ge concentration in the samples. In practice, the natural concentration of Ge was estimated by using the average Ge/Si ratio for seawater and known Si concentrations (or water depth). The double-spike was added to the acidified seawater samples and left to equilibrate for at least 2 hours. Experiments done with longer equilibration time revealed no effect on the isotopic value or Ge recovery.

About 4 mL of Fe(III) solution at 12,000 ppm Fe was added per liter of seawater, in order to obtain a final solution of about 12 mg Fe/L, and left to equilibrate for two hours. The solution pH was then increased to pH 8 ± 0.3 with concentrated optima-grade ammonia (NH_4OH) solution at 14M. Germanium co-precipitation with Fe hydroxides is achieved after 100 min (Pokrovsky et al., 2006). Analytical-grade NaOH solution at 8M was used in the initial stage of the experimental development but was discontinued due to significant blank contribution. A contamination of Ge in the NaOH pellets was suspected. The solution was left for at least 12 hours to flocculate. Then, the supernatant was siphoned off and the remaining slurry was transferred into 50mL centrifuge tubes. Fe-oxyhydroxide precipitates were finally recovered after centrifugation at 1500G for 4 minutes. The solid residue was then processed as other mineral or biogenic opal samples as described below.

2.4. Sponge spicule preparation

Preparation of the modern sponge spicules followed the protocol described in Hendry et al. (2010) for the measurements of Si isotopes, and was carried out in the Department of Earth Sciences, Oxford University. The modern spicules were initially separated from organic matter by repeatedly heating and sonicating in concentrated HNO_3 and 30 % H_2O_2. Sediment grains were removed by picking until visual inspection showed the spicules to be clear of detritus. The spicules were then additionally cleaned of any remaining organic matter and surface contaminants using three steps: 1) reductive cleaning using hydroxylamine chloride (0.1 %)/acetic acid solution (1 %), 2) etching with sodium fluoride (0.1 % NaF) and 3) oxidation with a strong acid solution (50 % HNO_3:HCl, in-house distilled) following previous methods (Ellwood et al., 2006).

2.5. Digestion and chromatographic separation

The method used in this study was derived from that used for Ge isotope analysis in rocks and minerals developed in Rouxel et al. (2006). Both Fe-oxyhydroxide precipitates and biogenic opal (avg. 50 and 25 mg, respectively) were dissolved with 1 mL of concentrated HF in Teflon beaker, after addition of an appropriate quantity of Ge double-spike in the case of biogenic opal. Samples were left for 2 hours on a hotplate at 90°C until dissolution was complete. The samples were then left to cool at room temperature and then diluted to 1 M HF using Milli-Q water.

An anion-exchange resin (AG1-X8, Bio-Rad, Hercules, CA, USA) was used for the separation of Ge from Fe and other matrix elements and isobaric interferences that could form volatile hydride (e.g. Se). A total of 24 LDPE columns were filled with 1.8 mL of resin (wet volume) and cleaned with 10 mL washes of 3M HNO_3, 0.28M HNO_3 and Milli-Q water, before being conditioned with 5 mL of 1M HF. The sample was loaded and fluorinated Ge was strongly adsorbed on the resin. 5 mL of 1M HF was used to elute most of the elements of the initial matrix followed by 3mL of Milli-Q water. Finally, Ge was eluted with 10mL of 0.28M HNO_3. The solution was recovered, evaporated to dryness on a hotplate at 80°C and re-dissolved in a precise volume of 0.28M HNO_3 so that all samples attained an identical final Ge concentration (typically 5ppb) for isotope analysis by hydride generation MC-ICP-MS.

2.6. Hydride generation (HG) MC-ICP-MS analysis

All measurements were carried out on a Thermo Scientific instrument MC-ICP-MS Neptune (PSO-IFREMER) with similar operating conditions as described in Escoube et al. (2012). An online hydride generation system (CETAC, HGX-200) was used to generate Ge hydride by mixing the Ge sample solution with $NaBH_4$ solution. This system is similar to previous studies (Rouxel et al., 2006) as it used two Argon inlets to transport Ge hydride and stabilize signal intensity, and an on-line PTFE filter to prevent aerosols from reaching the plasma. The sample and $NaBH_4$ solutions were introduced at the same flow rate of about 150 µl/min and were mixed in a 10 cm-long reaction coil before entering the gas-liquid separator.

The Neptune instrument was operated in low mass resolution mode, and ^{70}Ge, ^{72}Ge, ^{73}Ge and ^{74}Ge were measured on L2, C, H1 and H2 cups, whilst ^{68}Zn, ^{69}Ga, ^{71}Ga and ^{77}Se were also monitored on L4, L3, L1 and H4 cups. The isotope ^{76}Ge was not measured because of a major interference from $^{38}Ar_2$. The NIST 3120a standard solution was measured with the same instrumental set-up before and after each sample analysis. Each analysis consisted of 5 blocks of 6 measurements (2 seconds integration time per measurement). The Ge isotope composition of each block of measurements was calculated using the double-spike data reduction scheme presented in Siebert et al. (2001) for Mo isotopes. Data for each sample were then processed by removing the 5 % most extreme $\delta^{74/70}Ge$ values (outside 2SD) and normalized to average NIST 3120a values measured before and after the sample. The internal error was reported as two standard errors ($2SD/\sqrt{n}$) calculated using 5 blocks of 6 measurements each. External precision (as 2SD) of the sample was determined by calculating the standard deviation of all NIST 3120a standards measured during the same analytical session.

3. Results

3.1. Procedural blank and Ge recovery from seawater

During the initial stage of the analytical development, we observed significant contamination of the pure Fe(III) salt used for Ge co-precipitation of approximately 0.1 ng Ge per mg of Fe. Considering that up to 200 mg of Fe(III) was used per sample, this level of Ge blank precluded the analysis of Ge-depleted surface seawater. After further evaporation of the Fe(III) solution in 6 M HCl, Ge blanks were lowered to 0.01 ng/mg Fe. The procedural blanks were determined for each sample set by processing 1 to 4L of spiked ultrapure water

as an unknown sample. We determined an overall procedural blank ranging from 0.5 ng to as low as 0.1 ng, which may be either resulting from Ge impurities in both the Fe(III) solution and the NaOH or NH_4OH used to raise the pH for the co-precipitation step. This corresponds to an equivalent Ge concentration in seawater of 4L-size seawater ranging from 1.8 pM to 0.2 pM. By comparison, Ge blanks determined for the chromatographic separation only were below the detection limit of 0.01 ng, and therefore negligible. For surface seawater, the total amount of Ge recovered from a 4L-size sample was about 6 ng, so a maximum of 0.5 ng blank would correspond to up to 25 % of the measured signal, which requires careful examination of its effect on Ge isotope composition. Several lines of evidences suggest that blank contamination did not affect significantly our surface seawater measurement within analytical uncertainty. First, the comparison between surface and deep seawater at BATS (Table 1) and deep Pacific seawater yielded similar $\delta^{74/70}$Ge at 3.1 ± 0.3 ‰ despite significant concentration differences (from 7pM to 117 pM). We also did not observe any positive correlation between Ge/Si and Ge concentration in Ge-depleted surface seawater (Table 2), which would be expected if significant amounts of Ge were derived from blank contamination. We also attempted to measure the Ge isotope composition of the procedural blank and obtained a $\delta^{74/70}$Ge value of 1.6 ± 0.2 ‰ for Ge quantity of 0.4 ng, which is within the range of natural Ge composition (e.g. between crustal and seawater values). For deep seawater with Ge concentrations above 50 pM, the blanks were in all cases negligible with a contribution of less than 3 % of the total measured signal.

Although the use of Ge double-spike should correct for potential Ge isotope mass fractionation in the case of incomplete recovery, we evaluated a range of co-precipitation conditions in order to optimize Ge recovery and decrease the overall sample size. It is expected that the recovery yield of Ge using the Fe co-precipitation technique would be dependent on the final sample pH, the amount of Fe-oxyhydroxide in suspension, and the overall kinetics of Ge adsorption. Figure 2 presents the effect of pH and different iron additions on the Ge yield. Maximum adsorption of Ge occurred between pH 6 and 8, regardless of the quantity of Fe(III) added to seawater. These results are generally consistent with the study of Pokrovsky et al. (2006), who found a maximum adsorption of Ge at pH between 6 and 9. However, the yields were lower in our study, and ranged from 70% to > 90 % which is probably explained by the much lower Fe concentration (i.e. about 1000-fold) used for Fe coprecipitation compared to the experimental study of Pokrovsky et al. (2006). Iron oxides are also known to co-precipitate a range of trace elements including oxyanions

and trace metals (e.g. Martinez and McBride, 1998; Raven et al., 1998). Although competition between germanium and other solutes may occur during co-precipitation, we found no significant correlation between yield and nutrient concentrations or depth.

3.2. Determination of analytical accuracy and potential effects of methylated Ge species

We evaluated the accuracy of the analytical procedure using a standard addition method, similar to Rouxel et al. (2006), whereby incremental quantities of the Ge isotope standard was added to an unknown sample. This method allows the robust determination of the Ge concentration and Ge isotope composition of an unknown sample, and whether any changes in the initial matrix-to-analyte ratio causes any analytical artifacts or residual interferences. We used several aliquots of our internal seawater samples from the Bay of Brest, which were doped with various amounts of the Ge NIST 3120a standard. The composite samples were spiked and processed through the same chemical procedure as unknown samples. The Ge concentration and Ge isotope composition of these composite samples are presented in Fig. 3 along with two independent measurements of the pure seawater sample. The relationship between $\delta^{74/70}$Ge and Ge concentration values for the composite sample and the percentage of Ge added follows the predicted mixing relationship, with a $\delta^{74/70}$Ge value for Bay of Brest surface water estimated at 2.54 ± 0.41 ‰ (2SE) and with a Ge concentration of 7.4 ± 0.8 pM (2SE). By comparison, the two independent Ge isotopic measurements of Bay of Brest yielded $\delta^{74/70}$Ge value of 2.42 ± 0.07 ‰ (2SE) and 2.27 ± 0.16 ‰ (2SE), which are indistinguishable within uncertainty of the calculated value above, thus confirming the accuracy of the method.

Because organometallic Ge species exist in seawater in methyl-Ge (MMGe) and dimethyl-Ge (DMGe) forms (Lewis et al., 1985; Lewis et al., 1989), representing more than 70 % of the total Ge in the ocean, care should be taken to avoid the recovery of these species during chemical preconcentration of inorganic Ge. The vertical profiles of MMGe and DMGe in seawater typically show vertically homogeneous concentrations for both species within analytical error of 340 ± 7 pM MMGe and 110 ± 3 pM DMGe (Lewis et al., 1985). Hence, the sum of methylated Ge species in our surface seawater sample from the Bay of Brest is expected to be about 450 pM, which is several orders of magnitude higher than the measured inorganic Ge concentration of 7.4 pM. In spite of their higher abundances, methylated Ge species are unlikely to have co-precipitated with inorganic Ge considering their apparent absence of reactivity in a wide range of biogeochemical processes (Lewis et

al.,1985), including during early diagenesis leading to inorganic Ge sequestration in Fe-rich marine sediments (King et al., 2000). This situation may be different using other analytical methods involving the generation of volatile Ge hydride directly from seawater (Hambrick et al., 1984). Considering that methylated (i.e. organically-bound) Ge species should have much lighter Ge isotope composition than inorganic Ge species (Li et al., 2009), it is conceivable that the slightly lighter value obtained for the Bay of Brest ($\delta^{74/70}$Ge = 2.4 ‰) compared to deep oceanic waters ($\delta^{74/70}$Ge = 3.1 ‰, see below) could reflect a small proportion of methylated species in our measurements. However, the comparison between surface and deep seawater at BATS (Table 1) yielded similar $\delta^{74/70}$Ge values at about 3.0 ± 0.1 ‰ despite significant concentration differences (7pM to 24 pM). Hence, using a simple mass balance consideration, it is unlikely that methylated Ge species have any influence on the measurement of inorganic Ge species. Moreover, Baronas et al. (2017) recently performed a seawater Ge isotopic analyses separating inorganic Ge from methylated Ge using a liquid nitrogen trapping technique and they obtained similar results for deep seawater at BATS.

Finally, it is unlikely that any significant amount of methylated Ge species was converted to inorganic Ge during extended sample storage or exchanged isotopically with the Ge double spike. Lewis et al. (1985) reported that MMGe and DMGe can be converted to inorganic Ge by strong ultraviolet radiation only in freshwater medium, but not in seawater, which confirmed the apparent stability of these compounds during sample storage, even in acidic conditions. Previous studies (Mortlock and Froelich, 1996) have also demonstrated that organogermanium species do not exchange with the inorganic Ge spike under similar analytical conditions and equilibration time than in our study. Consequently, the methylated Ge species are ignored in the present paper and Ge is used to indicate only the inorganic form (predominantly germanic acid).

3.3. Seawater samples from the Atlantic and Pacific oceans

Germanium concentrations and isotopic compositions of the surface (GSI) and deep (GDI) seawater samples from the GEOTRACES IC1 BATS Atlantic intercalibration station (31°40′N 64°10′W) are presented in Table 1. For GS we obtained Ge = 7 pM and $\delta^{74/70}$Ge = 3.09 ± 0.26 (2SE). For GD we obtained Ge = 24 pM and $\delta^{74/70}$Ge = 2.89 ± 0.26 (2SE). By comparison, Froelich et al. (1985a) reported inorganic Ge concentrations of 3.5 pM and 15.6 pM, respectively, in surface (10 m) and deep (2000 m) seawater of the Sargasso Sea. Hence Ge concentrations are significantly higher than previously reported. It is possible that such

increase in Ge concentrations in surface seawater is related to the location of the BATS station near Bermuda, which is a region with typically high seasonal dust deposition. This hypothesis is supported by the fact that GSI and GDI have also relatively high Fe concentrations (0.42 and 0.84 nM, respectively) compared to open seawater where dust supply is more limited (Boyle et al., 2012; John and Adkins, 2012). For example, Fe concentrations as low as 0.02 nM (20 times less than the present surface sample) have been documented in the eastern Atlantic Ocean (Sarthou et al., 2003). On the other hand, if significant contamination (i.e. analytical bias) contributed to the increase of Ge concentration in surface seawater, the contaminant would need to have the same isotope composition (i.e. $\delta^{74/70}$Ge ≈ 3.0 ‰) as the average seawater value, which is quite unlikely considering that Ge in crustal materials has much lighter $\delta^{74/70}$Ge (~ 0.7 ‰, Rouxel et al., 2006; Escoube et al., 2012) and our single measurement of procedural blank yielding $\delta^{74/70}$Ge ~ 1.6 ‰.

Seawater samples from the Pacific Ocean located SW of Hawaii (FeMo Deep station) and nearby Loihi Seamount show remarkable homogeneity in $\delta^{74/70}$Ge and Ge concentrations (Table 1). A comparison between unfiltered and filtered samples show a difference of less than 2 % in Ge concentrations and less than 0.3 ‰ in $\delta^{74/70}$Ge values - both being close to the analytical uncertainties. Considering that both filtered and unfiltered samples were stored acidified to pH 1.8 for several months, these results suggest that Ge occurs essentially in the dissolved form at these water depths (i.e. between 959 to 3497 m). Considering the entire dataset obtained for the composite samples recovered during cruise Loihi 2014, we obtained average values of $\delta^{74/70}$Ge = 3.18 ± 0.32 ‰ (2SD, n=8) and Ge = 101 ± 18pM (2SD, n = 8). These measured Ge concentrations are indistinguishable from previously reported values for the deep Pacific Ocean (Froelich et al., 1985a; Mortlock et al., 1993). Filtered samples from the FeMo Deep station (Table 1) recovered at 500 m and 4000-4900 m depths yielded $\delta^{74/70}$Ge = 3.13 ± 0.11 ‰ and 3.27 ± 0.06 ‰ respectively, confirming the homogeneity of Ge isotope composition in the deep Pacific Ocean. As expected, the Ge concentration of 86 pM obtained at 500 m depth is lower than that for deeper water (> 4000 m, Ge ≈ 117 pM), again consistent with previous studies (Froelich et al., 1985a; Mortlock et al., 1993).

3.4. Seawater profiles from the Southern Ocean

Germanium concentrations and isotope compositions at the three stations in the Southern Ocean (Sars, WAP and Burdwood Bank) are reported in Fig. 4, 5 and 6. Germanium and Si concentrations show typical nutrient-type profiles, with lower Ge concentrations (down to 15 pM) in surface waters, increasing with depth up to 106 pM below 1000 m. Station WAP shows steeper gradients in Ge, Si and other nutrient at mid water depth compared to the other stations (Fig. 5). Using the relationship between Ge and Si concentrations (Fig. 7), we obtained an average Ge/Si ratio of 0.775± 0.036 (μmol/mol) which is consistent within our error to the global oceanic Ge/Si ratio of 0.760 ± 0.004 (μmol/mol) determined by Sutton et al. (2010). A plot of Ge versus Si concentration produced an intercept of 3.6 ± 3.3 pM, which is higher but also within error of the intercept of 1.27 ± 0.24 pM reported previously using a much larger dataset (Sutton et al., 2010).

The Ge isotopic profiles at Sars and WAP show distinct features. Firstly, surface waters are characterized by the heaviest $\delta^{74/70}$Ge values at ~ 3.5 to 3.7 ‰. Secondly, a minimum of $\delta^{74/70}$Ge is observed at mid-water depths, between 500 and 1000 m. Below 1000 m, $\delta^{74/70}$Ge values remain relatively constant at both stations, yielding an average of 3.17 ± 0.19 ‰ (2SD, n = 7) and 3.21 ± 0.21 ‰ (2SD, n = 5) for Sars and WAP respectively. Ge isotope compositions at the Burdwood Bank station also fall within a range of ~ 2.9 to 3.3 ‰, except for a single sample at 3250 m that show lighter $\delta^{74/70}$Ge at ~ 2.4 ‰.

3.5. Germanium/Silicon and Ge isotope composition of deep sea sponges

Modern sponges from the Southern Ocean present $\delta^{74/70}$Ge values ranging from 1.79 to 2.45 ‰ in agreement with previously reported $\delta^{74/70}$Ge values of Pacific Ocean sponges (Rouxel et al., 2006). The dataset include different species of demosponges (Demospongiae) and glass-sponges (Hexactinellida) sampled at water depths of 600 to 2266 m. As presented in Fig. 8, no systematic relationship between $\delta^{74/70}$Ge values and other parameters could be identified. In particular, we did not find an inverse linear relationship between sponge $\delta^{74/70}$Ge and [Si], which has been previously reported for δ^{30}Si and [Si] (Hendry et al., 2010). Compared to overlying seawater, sponges are fractionated toward light Ge isotopes, with a Ge isotope fractionation factor $\Delta^{74/70}Ge_{opal\text{-}SW}$ ranging from -0.57 to -1.21 ‰ and averaging -0.87 ± 0.37 ‰ (2SD, n = 12). Germanium concentrations ranged from 0.13 to 0.35 ppm, corresponding to Ge/Si ratios of 0.11 to 0.30 μmol/mol, which is much lower than the

446 modern seawater Ge/Si ratio of 0.7 μmol/mol and consistent with previous studies (Ellwood
447 et al., 2006; Rouxel et al., 2006).
448
449 **4. Discussion**
450
451 *4.1. Germanium isotope systematics in the Southern Ocean*
452
453 The Southern ocean is a complex zone where the mixing of waters from three oceans
454 occurs. The modern day Southern Ocean has large [Si] gradients, with [Si] increasing
455 polewards and with depth due to a combination of water mass mixing, a sloping isopycnal,
456 and opal remineralization (Pollard et al., 2002). The Southern Ocean plays an important role
457 in marine carbon exchange due to high primary productivity and the formation of deep waters
458 with high preformed nutrients (Nelson et al., 1995; Sarmiento et al., 2004). The water masses
459 in the Drake Passage are well known (Orsi et al., 1995; Orsi et al., 1999; Meredith et al.,
460 2011) and include: Antarctic Surface Water (AASW), Antarctic Bottom Water (AABW),
461 Lower Circumpolar Deep Water (LCDW), Upper Circumpolar Deep Water (UCDW) and
462 Antarctic Intermediate Water (AAIW) (Fig. 9). The UCDW is characterized by an oxygen
463 minimum and nutrient maximum, while the LCDW is denser (S_{max} = 34.7) and penetrates
464 south of the Antarctic Circumpolar Current (ACC) into the subpolar regime underneath the
465 AASW, i.e. below direct surface influence and characterized by a subsurface temperature
466 minimum. The UCDW spreads poleward and often reaches the Antarctic continental shelves.
467 The WAP station is separated from the Sars and Burdwood Bank stations by the polar
468 front (PF). Burdwood Bank is characterized by an important influence of the AAIW, which
469 provides oxygen to 1000m depth, and an oxygen minimum that is pronounced from 1200m to
470 2000m (Key *et al.*, 2004). The Sars and WAP off slope stations both have oxygen minima at
471 800m depth. There is an influence of LCDW from 1800m to the bottom, which carries
472 oxygen at depth to the Sars station (Key et al., 2004). A comparison between the $\delta^{74/70}$Ge of
473 dissolved inorganic Ge and oceanographic parameters (e.g. fluorescence, salinity-
474 temperature) at the three stations do not show systematic relationships, suggesting, as a
475 whole, that the different water masses of the Southern Ocean have relatively similar Ge
476 isotope compositions. This contrasts with Si isotope systematics of the Southern Ocean,
477 which are characterized by distinct δ^{30}Si signatures in the different water masses (Fripiat et

al., 2011). Considering that the residence time of Ge is probably shorter than that of Si (between 10,000 to 17,000 years, Treguer and De La Rocha, 2013), heterogeneity in Ge isotope composition between different water masses should be expected.

In detail, there is indeed some distinct Ge isotope variability in the water column profiles. We observed that the lowest $\delta^{74/70}$Ge values tend to be related to UCDW and LCDW (minimum of 2.62 and 2.44 ‰ respectively) while the heaviest deep water values were observed for the AABW (range of 2.97 to 3.32 ‰). The larger variations of $\delta^{74/70}$Ge at the Sars station are also observed at the interface between AAIW and LCDW. In the Burdwood Bank water column data, significant variations of $\delta^{74/70}$Ge are also observed at the interface between AAIW and UCDW. For both Sars and WAP profiles, the heaviest $\delta^{74/70}$Ge values, up to ~ 3.7 ‰ and ~ 3.5 ‰, are systematically observed in the shallowest sample (part of AAIW), coinciding with the samples with the highest fluorescence (Table 2). Hence, it can be suggested that the concomitant increase of $\delta^{74/70}$Ge and depletion of Ge in surface seawater at Sars may be related to phytoplankton biomass, and therefore explained by biological uptake. We note, however, that higher sample resolution may be needed to fully resolve the apparent relationships between Ge isotope fractionation and the deep chlorophyll maximum for this ocean region. Depth profiles at Sars also show a subsurface maximum of Ge/Si, which may result from Ge/Si fractionation during Si uptake (Murnane and Stallard, 1988; Froelich et al., 1989; Ellwood and Maher, 2003; Sutton et al., 2010). In Fig. 10, $\delta^{74/70}$Ge versus Ge concentrations are reported for the stations where surface seawater was sampled (i.e. Sars and WAP). Following the approach previously used for Si isotopes (De La Rocha et al., 1997), we modeled the variations of $\delta^{74/70}$Ge versus Ge using a Rayleigh distillation model, considering deep values (i.e. > 1000 m) of Ge = 110 pM. Model results for the uppermost water (> 1000 m) at the Sars station suggest that surface seawater values can be explained by a fractionation factor $\alpha_{seawater\text{-}diatom}$ of 1.00068 ± 0.00009 and initial water $\delta^{74/70}$Ge values of 2.26 ± 0.11 ‰. This model, however, cannot be extrapolated to deeper waters (>1300 m), which are characterized by heavier $\delta^{74/70}$Ge values at 3.1 ‰ (Fig. 10). It is also unlikely that Si and Ge in these surface waters were sourced from above 1300 m. Hence, biological removal of Ge in surface waters may not be the sole mechanism explaining the observed water column variations of both Ge concentrations and isotopic compositions at Sars. For the WAP station, the fractionation factor is closer to unity with $\alpha_{seawater\text{-}diatom}$ of □□□□□□□± 0.00011, with initial water $\delta^{74/70}$Ge value of 3.1 ± 0.05 ‰.

We now further evaluate whether subsurface water mixing could, instead, explain most of the variability observed in Sars and other stations. In particular, the minimum $\delta^{74/70}Ge \approx 2.6$ ‰ at Sars may suggest the presence of isotopically lighter water masses located at the interface between AAIW and LCDW. Klunder et al. (2014) observed an input of dissolved iron (DFe) from the shelves around Elephant Island into the Drake Passage, which is consistent with earlier findings (Dulaiova et al., 2009). Hence, we propose that similar shelf input may, in principle, contribute to lower $\delta^{74/70}Ge$ values, shifting deeper water (500-1000 m depth) from typical deepwater $\delta^{74/70}Ge$ values of 3.1 ‰ toward more crustal values at around 0.7 ‰. However, since DFe concentrations were not measured in the same samples as our new Ge data, it is difficult to further test this hypothesis. Considering the different reactivity and residence time of Fe and Ge, it is also possible that the same water column anomaly may not be observed for both elements in a similar manner. Higher resolution sampling, together with measurements of other important nutrients such as PO_4 and Fe, should ultimately allow us to determine the relative importance of the two mechanisms, driven by differential depth regeneration and/or shelf input, for Ge isotope variations in water column profiles.

Far-field hydrothermal venting from the South East Pacific Rise (Well et al., 2003), the Bransfield Strait (Klinkhammer et al., 2001) and the East Scotia Ridge back-arc basin (James et al., 2014) may also potentially impact Ge geochemistry in the region. However, the ≈ 0.5 ‰ shift observed for $\delta^{74/70}Ge$ values at 3251 m depth at the Burdwood Bank station is unlikely to result from the contribution of isotopically light hydrothermally-derived Ge (Escoube et al., 2015). In particular, any significant hydrothermal contribution would have been reflected in elevated ^{3}He concentrations which was not observed in this region (Sudre et al., 2011) or an increase in Ge/Si ratios at the same depth which was not observed either (Table 2).

4.2. Potential mechanisms of Ge isotope fractionation by siliceous phytoplankton

Our water column concentration and isotopic composition profiles exhibit distinct trends towards lower [Ge] and heavier $\delta^{74/70}Ge$ values at shallower depths (Fig. 4-6, 10), indicating that it is possible that Ge isotopes are fractionated during phytoplankton uptake by 0.3 ‰ to 0.6 ‰. Such biological fractionation could arise as a result of Ge uptake and

incorporation into diatom opal, or as a result of incorporation of Ge into organic matter within phytoplankton cells. We explore here the potential mechanisms leading to, or inversely muting, Ge/Si and Ge isotope fractionations by phytoplankton.

In a reconnaissance study, Mantoura (2006) reported the experimental determination of Ge isotope fractionation during biological uptake by two marine diatoms, *Skeletonema costatum* and *Thalassiosira weissflogii*. Neither of these species appeared to fractionate Ge isotopes during biomineralization of opal. These results were obtained across a wide range of Ge/Si in the culture media. There was no change in measured $\delta^{74/70}$Ge values of opal within the analytical precision of 0.3 ‰, even for Si depletion in solution up to 25 %. Since experiments were not run at higher percentages of Si uptake, it remains unclear as to whether Rayleigh-type fractionation behavior could lead to resolvable seawater $\delta^{74/70}$Ge variations. These diatom species are also not representative of the dominant sub-polar taxa in the Southern Ocean (Crosta et al., 2005) and we cannot rule out potential species-dependent Ge isotope fractionation by marine diatoms as previously reported for Si isotopes (Sutton et al., 2013). An important result, however, is that Ge isotope composition measured in uncleaned diatoms, i.e. whole diatom including organic matter and opal, yielded a fractionation factor $\alpha_{seawater\text{-}diatom} = 1.001 \pm 0.0004$ (2SD) (Mantoura, 2006). Hence, considering the strong affinity of Ge for organic matter, Ge sequestration in phytoplankton cellular material during biological uptake may provide a pool of isotopically light Ge that could be decoupled from Ge in opal at depth during remineralization, resulting in heavier $\delta^{74/70}$Ge values in surface waters (up to ~ 3.7 ‰). Evidence that Ge isotope distributions may be driven by organic matter remineralization is provided by our water column depth profiles, which show a correspondence between apparent oxygen utilization (AOU) — a measure of cellular material degradation — and seawater $\delta^{74/70}$Ge (Fig. 4 - 6). For example, a local minimum in $\delta^{74/70}$Ge is observed at the same depth as the AOU maximum at ~ 800 m at Sars (Fig. 4) with $\delta^{74/70}$Ge values as low as ~ 2.6 ‰, which is likely the result of the release of light Ge isotopes during the remineralization of settling organic matter. The same relationships were however not observed at WAP off slope (Fig. 5) and Burdwood Bank (Fig. 6). Considering that seawater samples at the three Southern Ocean stations were recovered during the austral fall 2011, when sea surface temperatures were already low (2.81 and -0.15 °C, at stations Sars and WAP, respectively), the concept of AOU should be used with caution. In particular, it has been shown that O_2 concentration can be significantly depleted under the ice due to incomplete equilibration with atmosphere (Gordon et al., 1984), providing a possible

explanation for the lack of relationships between $\delta^{74/70}$Ge and AOU at WAP off slope and Burdwood Bank.

4.3. Germanium isotope fractionation by sponges

In a preliminary study, Rouxel et al. (2006) reported heavy Ge isotope compositions relative to bulk oceanic-continental crust for opal sponge spicules obtained from live specimens growing on the seafloor in North East Pacific, with $\delta^{74/70}$Ge values ranging from 1.56 to 2.60 ‰ (recalculated relative to NIST 3120a). The new Ge isotope analysis of sponges from the Southern Ocean showed a similar, albeit smaller range from 1.79 to 2.45‰. Combining these results with $\delta^{74/70}$Ge values of overlying seawater, we determined a Ge isotope fractionation factor $\Delta^{74/70}Ge_{opal\text{-}SW}$ of -0.87 ± 0.37 ‰ (2SD, n = 12) during Ge uptake by sponges. Although no clear relationships could be derived between $\delta^{74/70}$Ge, water depth and oceanographic parameters (e.g. nutrient, temperature-salinity and AOU) or sponge species, these results confirm earlier assumptions that sponges fractionate Ge isotopes during biomineralization, and discriminate against heavy Ge isotopes, as already observed for Si isotopes (De La Rocha, 2003; Hendry and Robinson, 2012).

Sponges are considered to have a low affinity for silicic acid (Reincke and Barthel, 1997) and the inefficient silicon uptake mechanism has been suggested to explain their preferential enrichment in light Si isotopes (De La Rocha, 2003). More recently, Hendry et al. (2010) determined δ^{30}Si values of modern deep-sea sponge spicules and showed that they vary with ambient seawater Si concentrations. The fractionation factor $\Delta^{30}Si_{opal\text{-}SW}$ ranged from ca. -2.5 to -5.5 ‰ and showed a positive relationship with Si, which has been attributed to growth rate effects (Wille et al., 2010; Hendry and Robinson, 2012). However, no relationships between $\delta^{74/70}$Ge and δ^{30}Si, $\Delta^{30}Si_{opal\text{-}SW}$, nor Si concentrations could be identified (Fig. 8), suggesting a significant decoupling between Ge and Si isotopes during sponge biomineralization.

Biosilicification in sponges is controlled by two enzymes: silicatein, which promotes condensation reactions, and silicase, which dissolves silica (Muller et al., 2007). Although it is still unclear which pathways or reactions during the biosilicification process result in Si isotopic fractionation, our results show that Ge incorporation in sponges likely proceeds via a different pathways than Si. The non-linear relationship between Si isotope fractionation and silicon concentration has been modeled assuming that the fractionation occurs in several

steps: firstly as the Si is transported into the cell, secondly as the Si is polymerized, and thirdly as Si is lost from the cell (Wille et al., 2010; Hendry and Robinson, 2012). This model indicates that Si isotope fractionation associated with uptake transport is constant whereas fractionation during spicule formation increases as a function of external Si concentration. Using this model, we propose that the lack of correlation between $\Delta^{74/70}Ge_{opal\text{-}SW}$ and $\Delta^{30}Si_{opal\text{-}SW}$ may suggest that Ge isotopes are fractionated solely during the uptake step (i.e. which is also associated with constant Si isotope fractionation). Silicification of large spicules occurs extracellularly in association with an organic matrix and is controlled by protein interactions (Schröder et al., 2008). It is therefore likely that the apparent $\Delta^{74/70}Ge_{opal\text{-}SW}$ of -0.87 ‰ result from the interaction of $Ge(OH)_4$ with organic compounds, possibly through the formation of 6-coordinated Ge bearing organic complexes which may be enriched in light isotopes by up to 4 ‰ at 25 °C relative to $Ge(OH)_4$ (Li et al., 2009).

Measurements of Ge/Si ratios in sponge opal range from 0.11 to 0.30 (μmol/mol), which is significantly lower than the seawater Ge/Si ratio of 0.76 μmol/mol. In a previous study, Ellwood et al. (2006) reported an even larger range of Ge/Si ratios, between about 0.075 to 0.380 μmol/mol, in sponge opal collected from a range of depths and locations. A correlation between Ge/Si_{sp} in sponge opal and Ge concentration in seawater was also reported, suggesting that either Ge/Si_{sp} is solely dependent on the Ge concentration of the surrounding seawater and is independent of the Si concentration of that seawater, or that Ge/Si_{sp} is the product of strong Ge/Si fractionation during both Ge and Si uptake from the seawater surrounding the sponge (Ellwood et al., 2006). Our results are broadly consistent, but further suggest that Ge/Si_{sp} is not solely a function of Ge concentration in seawater, since several samples deviate from the relationship reported by Ellwood et al. (2006) (Fig. 8). While Ge/Si and Ge isotope ratios in sponge opal do not appear to be species dependent (Fig. 8), sponges from the same area and the same species (e.g. sample DR13-47 and DR16-47) yielded contrasting $\delta^{74/70}$Ge and Ge/Si values, suggesting that vital effects between or within species may be significant in controlling both Ge isotope fractionation and Ge/Si ratios.

Although additional work is required, it seems likely that the same mechanisms leading to the discrimination of Ge against Si during biomineralization are also responsible for the fractionation of Ge isotopes. This hypothesis is supported by the fact that diatoms, which are known to produce subtle Ge/Si fractionation in surface waters (Sutton et al., 2010), also generate very limited Ge isotope fractionation. In contrast, marine sponges, which are characterized by Ge/Si values considerably lower than seawater, showed the largest Ge

isotope fractionation factors. This general model is also consistent with Si isotope systematics, i.e. sponges show larger degree of Si isotope fractionation than diatoms (De La Rocha et al., 1997; Wille et al., 2010).

4.4. A preliminary estimate of Ge isotope composition of seawater and implications for the global Ge budget

Results for the deep Pacific Ocean off Hawaii and deep Atlantic off Bermuda (BATS station) > 1000 m water depths show nearly identical $\delta^{74/70}$Ge of 3.19 ± 0.31 ‰ (2SD, n = 9) and 2.93 ± 0.10 ‰ (2SD, n = 2). Vertical distributions of Ge concentrations and isotope compositions in the Southern Ocean for water depths > 1300 m yielded an average $\delta^{74/70}$Ge value of 3.13 ± 0.2 5‰ (2SD, n = 14). These observations suggest that Ge isotope composition is relatively homogeneous in deep seawater and is not modified significantly through global thermohaline circulation and the biogenic uptake of dissolved silica. Hence, even with this relatively limited dataset, it is possible to determine a global deep seawater composition of approximately $\delta^{74/70}$Ge = 3.14 ± 0.38 ‰ (2SD, n = 27).

Mantoura (2006) investigated the Ge/Si and $\delta^{74/70}$Ge records of diatom opal from Late Quaternary sediments and found no difference between average glacial and average interglacial $\delta^{74/70}$Ge opal values. The average $\delta^{74/70}Ge_{opal}$ value over the period 68 to 178 ka (S. Atlantic, ODP site 1094) was determined to be 3.35 ± 0.29 ‰ (2SD, n = 29). Given that potential glacial-interglacial changes in $\delta^{74/70}Ge_{opal}$ are barely outside the analytical error, despite large changes in growth conditions, these initial results are fully consistent with our finding that diatom opal does not fractionate significantly Ge isotopes nor Ge/Si and thus might provide a potential paleoceanographic archive of secular Ge isotope variations in seawater.

Overall, our study supports the hypothesis that sedimentary diatomaceous sediments are potentially good archives for marine Ge biogeochemical cycling in the past. This new paleoceanographic tool could be applied to understand changes in hydrothermal versus continental Ge sources or Ge sinks over the past, considering the contrasting Ge isotope composition of hydrothermal vent fluids and Ge sinks related to Ge sequestration in Fe-rich sediments (see Escoube et al., 2015). The use of Ge isotopes seems also particularly relevant as a complementary tool for Si isotopes, especially if different water masses carry their own

672 $\delta^{74/70}$Ge signatures that are decoupled from their δ^{30}Si compositions. In this case, Ge isotopes
673 could provide additional information about the source of the water mass (and its potential
674 interaction with shelf environments), while Si isotopes would add additional information on
675 the operation of the biological pump. Surface seawater conditions are recorded in diatoms,
676 meaning that diatomaceous opal $\delta^{74/70}$Ge may trace nutrient sources (e.g. shelf input) and
677 their effect on primary productivity, while sponges provide information on deeper water (e.g.
678 hydrothermal input) and long-term oceanic circulation. Additional study of Ge isotope
679 systematics in coastal waters and rivers is now required to address the importance of
680 continental run-off and silicate weathering, as well as anthropogenic input (e.g. coal
681 combustion), in the marine biogeochemical cycling of Ge.
682
683 **5. Conclusion**
684 Prior to this study and the recent study of Baronas et al. (2017), our knowledge of Ge
685 isotope systematics in seawater was limited by the analytical difficulties to precisely measure
686 Ge isotope composition in sub-nanomolar amounts of Ge in seawater. Our newly developed
687 method offers the following advantages 1) utilization of a double-spike which permits
688 correction of potential Ge isotope mass fractionation in the case of incomplete recovery, 2)
689 sufficient sensitivity using hydride-generation system to measure Ge in seawater at very low
690 concentrations (e.g. surface waters), 3) a preconcentration technique using co-precipitation
691 with Fe-oxyhydroxides which can be set up on a research cruise, allowing the rapid
692 separation of Ge from large volumes of seawater. Additional developments are still required
693 to consistently achieve quantitative recovery (i.e. 100 % yield) of Ge from large seawater
694 volume. Potential blank contamination should also be kept at the minimum (i.e. below 1pM
695 equivalent) in order to improve the measurement of the most analytically challenging surface
696 seawater, especially from nutrient-depleted regions where significant Ge/Si fractionation is
697 expected. In this case, Ge isotope systematics may provide an important new proxy to
698 investigate nutrient limitation for biological productivity and their sources in surface
699 seawater, both of which resulting in contrasting trends in δ^{30}Si and Ge/Si ratios.
700 The first survey of Ge isotope systematics in seawater from the Pacific, Atlantic and
701 Southern Oceans indicates:
702 [1] Deep sea waters (<1000 m) are relatively homogeneous for the three Oceans with a
703 $\delta^{74/70}$Ge of 3.14 ± 0.38 ‰ (2SD, n = 27). This value is consistent with previous estimates of

704 $\delta^{74/70}$Ge values of seawater using biogenic opal (Mantoura, 2006; Escoube et al., 2015) and
705 recently reported by Baronas et al., (2017).

706 [2] $\delta^{74/70}$Ge profiles in the Southern Ocean show significant enrichment in heavy isotopes in
707 surface waters, while a minimum in $\delta^{74/70}$Ge is observed at the depth of maximum
708 remineralization. A combination of two different mechanisms can explain these profiles. The
709 first process may be driven by biology, namely the fractionation of Ge isotopes by siliceous
710 phytoplankton. Fractionation factors $\alpha_{\text{seawater-diatom}}$ during biological uptake into organic
711 matter were calculated with a Rayleigh distillation model that leads to values of 1.0007 (Sars)
712 and 1.0003 (WAP). Due to the strong affinity of Ge for organic matter, it is expected that the
713 light Ge isotopes may be incorporated in the soft tissues, leading to isotopically heavier
714 surface seawater compared to deeper seawater. Conversely, the remineralization of the
715 settling particles may be responsible for a decrease of $\delta^{74/70}$Ge values with depth
716 corresponding to AOU maximum. The second process is driven by physical mixing of water
717 masses. Although $\delta^{74/70}$Ge values are more homogeneous than δ^{30}Si between water masses,
718 significant variations can still be attributed to water masses having contrasting Ge isotope
719 signatures. Deep water masses forming close to the shelf are potentially lighter due to an
720 input of isotopically light lithogenic Ge. Because of the relatively limited number of sampling
721 depths and stations considered in this study, a distinction between these different mechanisms
722 remains difficult at this point. Future study should therefore be aimed at testing the relative
723 importance of internal cycling and source effects in controlling Ge isotope compositions in
724 seawater.

725 [3] The $\delta^{74/70}$Ge of sponges and co-located seawater allowed us to determine a Ge isotope
726 fractionation factor of -0.87 ± 0.37 ‰ (2SD, n = 12) during Ge uptake by sponges. Hence,
727 similarly to Si isotopes, sponges discriminate against heavy Ge isotopes during
728 biomineralization, suggesting that Ge isotopes could serve as an interesting biogeochemical
729 tracer when used in conjunction with Ge/Si and Si isotope systematics. In particular, the
730 apparent lack of correlation between Ge isotope compositions and Si (or Ge) concentrations
731 contrasts strongly with Si isotopes, allowing to use coupled $\delta^{74/70}$Ge and δ^{30}Si signatures in
732 sponges to reconstruct a paleoceanographic record of both silicic acid supply and utilization
733 (δ^{30}Si based proxy) and sources ($\delta^{74/70}$Ge based proxy) in seawater.

734 Finally, the apparent lack of Ge isotope and Ge/Si fractionation during diatom growth
735 remains an area of open research, given that significant fractionation is expected by analogy
736 with the widely investigated Si isotope systematics (De La Rocha et al., 1997; Sutton et al.,

737 2013). Since the extent of potential biological Ge isotope fractionation in surface seawater is
738 strongly model dependent, combined field studies at higher resolution profile and
739 experimental studies under conditions relevant to the ocean are now required to better
740 understand the biological imprint on the global Ge cycle.
741

Acknowledgements:

Support for Rouxel was provided by LabexMer ANR-10-LABX-19-01, Europole Mer and FP7 (#247837) grants. International mobility was provided to Guillermic by the LabexMer ANR-10-LABX-19-01 and the Royal Society (Hendry grant #UF120084). Jill Sutton is thanked for her advice. Emmanuel Ponzevera (IFREMER) and Yoan Germain (IFREMER) are thanked for their technical support, and Rosalind Rickaby (Univ. Oxford) is thanked for the generous use of laboratory space. Brian Glazer, Gabrielle Weiss, Angelos Hannides, Kristen Fogaren (Univ. Hawaii), and Isabelle Baconnais (Univ. Brest) are thanked for their support during cruise FK140626 aboard R/V Falkor. Southern Ocean water and sponge sample collection was funded by the National Science Foundation (OPP ANT grants #0944474 and #0902957; PIs Robinson and Waller). Samples from Loihi Seamount were collected as part of a project supported by the Schmidt Ocean Institute. We thank the crews of the R/V Nathaniel B. Palmer, R/V Kilo Moana, and R/V Falkor for assistance with deployments and sample collection during the cruises. We thank Jotautas Baronas, Michael Ellwood, AE Silke Severmann and one anonymous reviewer for their constructive reviews that improved the quality of this paper.

References

Baronas, J.J., Hammond, D.E., Berelson, W.M., McManus, J. and Severmann, S. (2016) Germanium-silicon fractionation in a river-influenced continental margin: The Northern Gulf of Mexico. *Geochim. Cosmochim. Acta* **178**, 124-142.

Baronas, J.J., Hammond, D.E., McManus, J., Wheat, C.G. and Siebert, C. (2017) A Global Ge Isotopic Budget. *Geochim. Cosmochim. Acta* **203**, 265-283.

Belissont, R., Boiron, M.C., Luais, B. and Cathelineau, M. (2014) LA-ICP-MS analyses of minor and trace elements and bulk Ge isotopes in zoned Ge-rich sphalerites from the Noailhac - Saint-Salvy deposit (France): Insights into incorporation mechanisms and ore deposition processes. *Geochim. Cosmochim. Acta* **126**, 518-540.

Bennett, S.A., Hansman, R.L., Sessions, A.L., Nakamura, K. and Edwards, K.J. (2011) Tracing iron-fueled microbial carbon production within the hydrothermal plume at the Loihi seamount. *Geochim. Cosmochim. Acta* **75**, 5526–5539.

Boyle, E.A., John, S., Abouchami, W., Adkins, J.F., Echegoyen-Sanz, Y., Ellwood, M., Flegal, A.R., Fornace, K., Gallon, C., Galer, S., Gault-Ringold, M., Lacan, F., Radic, A., Rehkämper, M., Rouxel, O., Sohrin, Y., Stirling, C., Thompson, C., Vance, D., Xue, Z.C. and Zhao, Y. (2012) GEOTRACES IC1 (BATS) contamination-prone trace element isotopes Cd, Fe, Pb, Zn, Cu, and Mo intercalibration. *Limnol Oceanogr-Meth* **10**, 653-665.

Cao, Z.M., Frank, M. and Dai, M.H. (2015) Dissolved silicon isotopic compositions in the East China Sea: Water mass mixing vs. biological fractionation. *Limnol. Oceanogr.* **60**, 1619-1633.

Crosta, X., Romero, O., Armand, L.K. and Pichon, J.J. (2005) The biogeography of major diatom taxa in Southern Ocean sediments: 2. Open ocean related species. *Palaeogeography Palaeoclimatology Palaeoecology* **223**, 66-92.

De La Rocha, C., Brzezinski, M.A. and De Niro, M.J. (1997) Fractionation of silicon isotopes by marine diatoms during biogenic silica formation. *Geochim. Cosmochim. Acta* **61**, 5051-5056.

De La Rocha, C. (2003) Silicon isotope fractionation by marine sponges and the reconstruction of the silicon isotope composition of ancient deep water. *Geology* **31**, 423-426.

de Souza, G.F., Slater, R.D., Dunne, J.P. and Sarmiento, J.L. (2014) Deconvolving the controls on the deep ocean's silicon stable isotope distribution. *Earth. Planet. Sci. Lett.* **398**, 66-76.

Dulaiova, H., Ardelan, M.V., Henderson, P.B. and Charette, M.A. (2009) Shelf-derived iron inputs drive biological productivity in the southern Drake Passage. *Global Biogeochem. Cycles* **23**.

Edwards, K.J., Glazer, B.T., Rouxel, O.J., Bach, W., Emerson, D., Davis, R.E., Toner, B.M., Chan, C.S., Tebo, B.M., Staudigel, H. and Moyer, C.L. (2011) Ultra-diffuse hydrothermal venting supports Fe-oxidizing bacteria and massive umber deposition at 5000 m off Hawaii. *Isme Journal* **5**, 1748-1758.

798 Ellwood, M.J. and Maher, W.A. (2003) Germanium cycling in the waters across a frontal
799 zone: the Chatham Rise, New Zealand. *Mar. Chem.* **80**, 145-159.

800 Ellwood, M.J., Kelly, M., Maher, W.A. and De Deckker, P. (2006) Germanium incorporation
801 into sponge spicules: Development of a proxy for reconstructing inorganic germanium and
802 silicon concentrations in seawater. *Earth. Planet. Sci. Lett.* **243**, 749-759.

803 Escoube, R., Rouxel, O.J., Luais, B., Ponzevera, E. and Donard, O.F.X. (2012) An
804 Intercomparison Study of the Germanium Isotope Composition of Geological Reference
805 Materials. *Geostand. Geoanal. Res.* **36**, 149-159.

806 Escoube, R., Rouxel, O., Edwards, K., Glazer, B. and Donard, O. (2015) Coupled Ge/Si and
807 Ge isotope ratios as geochemical tracers of seafloor hydrothermal systems: case studies at
808 Loihi Seamount and East Pacific Rise 9°50'N. *Geochim. Cosmochim. Acta* **167**, 93-112.

809 Fripiat, F., Cavagna, A.J., Dehairs, F., Speich, S., Andre, L. and Cardinal, D. (2011) Silicon
810 pool dynamics and biogenic silica export in the Southern Ocean inferred from Si-isotopes.
811 *Ocean Sci.* **7**, 533-547.

812 Froelich, P.N. and Andreae, M.O. (1981) The marine geochemistry of germanium -
813 Ekasilicon. *Science* **213**, 205-207.

814 Froelich, P.N., Hambrick, G.A., Andreae, M.O., Mortlock, R.A. and Edmond, J.M. (1985a)
815 The geochemistry of inorganic germanium in natural waters. *Journal of Geophysical*
816 *Research-Oceans* **90**, 1133-1141.

817 Froelich, P.N., Hambrick, G.A., Kaul, L.W., Byrd, J.T. and Lecointe, O. (1985b)
818 Geochemical behavior of inorganic germanium in an unperturbed estuary. *Geochim.*
819 *Cosmochim. Acta* **49**, 519-524.

820 Froelich, P.N., Mortlock, R.A. and Shemesh, A. (1989) Inorganic germanium and silica in the
821 Indian Ocean: Biological fractionation during (Ge/Si)OPAL formation. *Global Biogeochem.*
822 *Cycles*, **3**, 79–88.

823 Gordon, A.L., Chen, C.T.A. and Metcalf, W.G. (1984) Winter mixed layer entrainment of
824 Weddell Deep Water. *Journal of Geophysical Research-Oceans* **89**, 637-640.

825 Grasse, P., Ehlert, C. and Frank, M. (2013) The influence of water mass mixing on the
826 dissolved Si isotope composition in the Eastern Equatorial Pacific. *Earth. Planet. Sci. Lett.*
827 **380**, 60-71.

828 Hambrick, G.A., Froelich, P.N., Andreae, M.O. and Lewis, B.L. (1984) Determination of
829 methylgermanium species in natural waters by graphite furnace atomic absorption
830 spectrometry with hydride generation. *Anal Chem* **56**, 421-424.

831 Hammond, D.E., McManus, J., Berelson, W.M., Meredith, C., Klinkhammer, G.P. and Coale,
832 K.H. (2000) Diagenetic fractionation of Ge and Si in reducing sediments: The missing Ge
833 sink and a possible mechanism to cause glacial/interglacial variations in oceanic Ge/Si.
834 *Geochim. Cosmochim. Acta* **64**, 2453-2465.

Hendry, K.R., Georg, R.B., Rickaby, R.E.M., Robinson, L.F. and Halliday, A.N. (2010) Deep ocean nutrients during the Last Glacial Maximum deduced from sponge silicon isotopic compositions. *Earth. Planet. Sci. Lett.* **292**, 290-300.

Hendry, K.R. and Robinson, L.F. (2012) The relationship between silicon isotope fractionation in sponges and silicic acid concentration: Modern and core-top studies of biogenic opal. *Geochim. Cosmochim. Acta* **81**, 1-12.

Hendry, K.R. and Andersen, M.B. (2013) The zinc isotopic composition of siliceous marine sponges: Investigating nature's sediment traps. *Chem. Geol.* **354**, 33-41.

James, R.H., Green, D.R.H., Stock, M.J., Alker, B.J., Banerjee, N.R., Cole, C., German, C.R., Huvenne, V.A.I., Powell, A.M. and Connelly, D.P. (2014) Composition of hydrothermal fluids and mineralogy of associated chimney material on the East Scotia Ridge back-arc spreading centre. *Geochim. Cosmochim. Acta* **139**, 47-71.

John, S.G. and Adkins, J. (2012) The vertical distribution of iron stable isotopes in the North Atlantic near Bermuda. *Global Biogeochem. Cycles* **26**.

Kaya, M. and Volkan, M. (2011) Germanium determination by flame atomic absorption spectrometry: An increased vapor pressure-chloride generation system. *Talanta* **84**, 122-126.

King, S.L., Froelich, P.N. and Jahnke, R.A. (2000) Early diagenesis of germanium in sediments of the Antartic South Atlantic: In search of the missing Ge sink. *Geochim. Cosmochim. Acta* **64**, 1375-1390.

Klinkhammer, G.P., Chin, C.S., Keller, R.A., Dahlmann, A., Sahling, H., Sarthou, G., Petersen, S. and Smith, F. (2001) Discovery of new hydrothermal vent sites in Bransfield Strait, Antarctica. *Earth. Planet. Sci. Lett.* **193**, 395-407.

Klunder, M.B., Laan, P., De Baar, H.J.W., Middag, R., Neven, I. and Van Ooijen, J. (2014) Dissolved Fe across the Weddell Sea and Drake Passage: impact of DFe on nutrient uptake. *Biogeosciences* **11**, 651-669.

Kurtz, A.C., Derry, L.A. and Chadwick, O.A. (2002) Germanium-silicon fractionation in the weathering environment. *Geochim. Cosmochim. Acta* **66**, 1525-1537.

Kurtz, A.C., Lugolobi, F. and Salvucci, G. (2011) Germanium-silicon as a flow path tracer: Application to the Rio Icacos watershed. *Water Resour. Res.* **47**.

Lewis, B.L., Froelich, P.N. and Andreae, M.O. (1985) Methylgermanium in natural waters. *Nature* **313**, 303-305.

Lewis, B.L., Andreae, M.O. and Froelich, P.N. (1989) Sources and sinks of methylgermanium in natural waters. *Mar. Chem.* **27**, 179-200.

Li, X.F., Zhao, H., Tang, M. and Liu, Y. (2009) Theoretical prediction for several important equilibrium Ge isotope fractionation factors and geological implications. *Earth. Planet. Sci. Lett.* **287**, 1-11.

Luais, B. (2012) Germanium chemistry and MC-ICPMS isotopic measurements of Fe-Ni, Zn alloys and silicate matrices: Insights into deep Earth processes. *Chem. Geol.* **334**, 295-311.

873 Mantoura, S. (2006) Development and Application of Opal Based Paleoceanographic Proxies,
874 Univ. Cambridge. University of Cambridge, Cambridge, p. 218.

875 Martinez, C.E. and McBride, M.B. (1998) Coprecipitates of Cd, Cu, Pb and Zn in iron oxides:
876 Solid phase transformation and metal solubility after aging and thermal treatment. *Clays Clay*
877 *Miner.* **46**, 537-545.

878 McManus, J., Hammond, D.E., Cummins, K., Klinkhammer, G.P. and Berelson, W.M. (2003)
879 Diagenetic Ge-Si fractionation in continental margin environments: Further evidence for a
880 nonopal sink. *Geochim. Cosmochim. Acta* **67**, 4545-4557.

881 Meredith, M.P., Woodworth, P.L., Chereskin, T.K., Marshall, D.P., Allison, L.C., Bigg, G.R.,
882 Donohue, K., Heywood, K.J., Hughes, C.W., Hibbert, A., Hogg, A.M., Johnson, H.L., Jullion,
883 L., King, B.A., Leach, H., Lenn, Y.D., Maqueda, M.A.M., Munday, D.R., Garabato, A.C.N.,
884 Provost, C., Sallee, J.B. and Sprintall, J. (2011) Sustained monitoring of the Southern Ocean
885 at Drake Passage: Past achievements and future priorities. *Rev. Geophys.* **49**.

886 Mortlock, R.A. and Froelich, P.N. (1987) Continental weathering of germanium: Ge/Si in the
887 global discharge. *Geochim. Cosmochim. Acta* **51**, 2075-2082.

888 Mortlock, R.A., Froelich, P.N., Feely, R.A., Massoth, G.J., Butterfield, D.A. and Lupton, J.E.
889 (1993) Silica and germanium in Pacific Ocean hydrothermal vents and plumes. *Earth. Planet.*
890 *Sci. Lett.* **119**, 365-378.

891 Muller, W.E.G., Li, J.H., Schroder, H.C., Qiao, L. and Wang, X.H. (2007) The unique
892 skeleton of siliceous sponges (Porifera; Hexactinellida and Demospongiae) that evolved first
893 from the Urmetazoa during the Proterozoic: a review. *Biogeosciences* **4**, 219-232.

894 Murnane, R.J. and Stallard, R.F. (1988) Germanium/silicon fractionation during biogenic opal
895 formation. *Paleoceanography* **3**, 461-469.

896 Nelson, D.M., Treguer, P., Brzezinski, M.A., Leynaert, A. and Queguiner, B. (1995)
897 Production and dissolution of biogenic silica in the ocean: Revised global estimates,
898 comparison with regional data and relationship to biogenic sedimentation. *Global*
899 *Biogeochem. Cycles* **9**, 359-372.

900 Olbers, D., Gouretski, V.V., Seiß, G., Schröter, J., 1992. Southern Ocean Atlas (ODV).

901 Orsi, A.H., Whitworth, T. and Nowlin, W.D. (1995) On the meridional extent and fronts of
902 the Antarctic Circumpolar Current. *Deep-Sea Research Part I-Oceanographic Research*
903 *Papers* **42**, 641-673.

904 Orsi, A.H., Johnson, G.C. and Bullister, J.L. (1999) Circulation, mixing, and production of
905 Antarctic Bottom Water. *Prog. Oceanogr.* **43**, 55-109.

906 Pokrovski, G.S. and Schott, J. (1998) Experimental study of the complexation of silicon and
907 germanium with aqueous organic species: Implications for germanium and silicon transport
908 and Ge/Si ratio in natural waters. *Geochim. Cosmochim. Acta* **62**, 3413-3428.

909 Pokrovsky, O.S., Pokrovski, G.S., Schott, J. and Galy, A. (2006) Experimental study of
910 germanium adsorption on goethite and germanium coprecipitation with iron hydroxide: X-ray

absorption fine structure and macroscopic characterization. *Geochim. Cosmochim. Acta* **70**, 3325–3341.

Pollard, R.T., Lucas, M.I. and Read, J.F. (2002) Physical controls on biogeochemical zonation in the Southern Ocean. *Deep-Sea Research II* **49**, 3289–3305.

Qi, H.W., Rouxel, O., Hu, R.Z., Bi, X.W. and Wen, H.J. (2011) Germanium isotopic systematics in Ge-rich coal from the Lincang Ge deposit, Yunnan, Southwestern China. *Chem. Geol.* **286**, 252-265.

Raven, K.P., Jain, A. and Loeppert, R.H. (1998) Arsenite and arsenate adsorption on ferrihydrite: Kinetics, equilibrium, and adsorption envelopes. *Environ. Sci. Technol.* **32**, 344-349.

Reincke, T. and Barthel, D. (1997) Silica uptake kinetics of Halichondria panicea in Kiel Bight. *Mar. Biol.* **129**, 591-593.

Reynolds, B.C., Frank, M. and Halliday, A.N. (2006) Silicon isotope fractionation during nutrient utilization in the North Pacific. *Earth. Planet. Sci. Lett.* **244**, 431–443.

Rouxel, O., Galy, A. and Elderfield, H. (2006) Germanium isotopic variations in igneous rocks and marine sediments. *Geochim. Cosmochim. Acta* **70**, 3387-3400.

Robinson, L., (2015). Uncalibrated Hydrographic Data acquired with a CTD in the Drake Passage during the Nathaniel B. Palmer expedition NBP1103 (2011). Integrated Earth Data Applications (IEDA). doi: http://dx.doi.org/10.1594/IEDA/317657.

Sarmiento, J.L., Gruber, N., Brzezinski, M.A. and Dunne, J.P. (2004) High-latitude controls of thermocline nutrients and low latitude biological productivity. *Nature* **427**, 56-60.

Sarthou, G., Baker, A.R., Blain, S., Achterberg, E.P., Boye, M., Bowie, A.R., Croot, P., Laan, P., de Baar, H.J.W., Jickells, T.D. and Worsfold, P.J. (2003) Atmospheric iron deposition and sea-surface dissolved iron concentrations in the eastern Atlantic Ocean. *Deep-Sea Research Part I-Oceanographic Research Papers* **50**, 1339-1352.

Schlitzer, R., Ocean Data View, https://odv.awi.de, 2016.

Schröder, H.C., Wang, X.H., Tremel, W., Ushijima, H. and Muller, W.E.G. (2008) Biofabrication of biosilica-glass by living organisms. *Natural Product Reports* **25**, 455-474.

Siebert, C., Nagler, T.F. and Kramers, J.D. (2001) Determination of molybdenum isotope fractionation by double-spike multicollector inductively coupled plasma mass spectrometry. *Geochem Geophy Geosy* **2**, art. no.-2000GC000124.

Siebert, C., Ross, A. and McManus, J. (2006) Germanium isotope measurements of high-temperature geothermal fluids using double-spike hydride generation MC-ICP-MS. *Geochim. Cosmochim. Acta* **70**, 3986-3995.

Siebert, C., Hammond, D.E., Ross, A. and McManus, J. (2011) Germanium isotope measurements of high-temperature geothermal fluids using double-spike hydride generation MC-ICP-MS (vol 70, pg 3986, 2006). *Geochim. Cosmochim. Acta* **75**, 6267-6269.

948 Sudre, J., Garcon, V., Provost, C., Sennechael, N., Huhn, O. and Lacombe, M. (2011) Short-
949 term variations of deep water masses in Drake Passage revealed by a multiparametric analysis
950 of the ANT-XXIII/3 bottle data. *Deep-Sea Research Part Ii-Topical Studies in Oceanography*
951 **58**, 2592-2612.

952 Sutton, J., Ellwood, M.J., Maher, W.A. and Croot, P.L. (2010) Oceanic distribution of
953 inorganic germanium relative to silicon: Germanium discrimination by diatoms. *Global*
954 *Biogeochem. Cycles* **24**.

955 Sutton, J.N., Varela, D.E., Brzezinski, M.A. and Beucher, C.P. (2013) Species-dependent
956 silicon isotope fractionation by marine diatoms. *Geochim. Cosmochim. Acta* **104**, 300-309.

957 Treguer, P.J. and De La Rocha, C.L. (2013) The World Ocean Silica Cycle, in: Carlson, C.A.,
958 Giovannoni, S.J. (Eds.), Annual Review of Marine Science, Vol 5, pp. 477-501.

959 Well, R., Roether, W. and Stevens, D.P. (2003) An additional deep-water mass in Drake
960 Passage as revealed by He-3 data. *Deep-Sea Research Part I-Oceanographic Research*
961 *Papers* **50**, 1079-1098.

962 Wheat, C.G. and McManus, J. (2008) Germanium in mid-ocean ridge flank hydrothermal
963 fluids. *Geochem Geophy Geosy* **9**.

964 Wille, M., Sutton, J., Ellwood, M.J., Sambridge, M., Maher, W., Eggins, S. and Kelly, M.
965 (2010) Silicon isotopic fractionation in marine sponges: A new model for understanding
966 silicon isotopic variations in sponges. *Earth. Planet. Sci. Lett.* **292**, 281-289.

967

968

969

Figure captions

Figure 1: Map of the Southern Ocean and Drake Passage showing the location of hydrographic stations investigated for Ge concentration and isotope composition: Sars, WAP and Burdwood Bank. Location of deep sea sponges are also represented (see map caption). The locations of water mass fronts are from Orsi et al. (2015). The map was produced using Ocean Data view (Shlitzer, 2016).

Figure 2: Recovery yield of Ge by co-precipitation with Fe-oxyhydroxide as a function of pH and amount of Fe added (in mg) in seawater matrix. Experiments performed using filtered surface seawater from the Bay of Brest, with a total volume of 4 L for each experiments. Yield was determined by the amount of double-spike recovered and is therefore independent of blank and initial Ge present in the sample.

Figure 3: Ge concentration (squares) (a) and Ge isotope composition (squares) (b) of synthetic seawater samples obtained by doping surface coastal seawater (from Bay of Brest) with various amount of Ge standard SRM 3120a. The extrapolated $\delta^{74/70}$Ge value (circle) determined by the relationship in (b) is estimated to be 2.55 ± 0.41 ‰ (2SE), undistinguishable from duplicate measurement of un-doped "Bay of Brest" internal standards (triangles). Error bars show precision at 2SE and are often smaller than the datapoint symbol.

Figure 4: Vertical profiles of Ge isotope composition ($\delta^{74/70}$Ge), Ge concentration (in pM), Ge/Si ratios (μmol/mol) and apparent oxygen utilization (AOU) at station Sars, Southern Ocean. Dashed lines indicate the limits between the water masses, Antarctic Intermediate water (AAIW), Upper Circumpolar Deep Water (UCDW) and Low Circumpolar Deep Water (LCDW).

Figure 5: Vertical profiles of Ge isotope composition ($\delta^{74/70}$Ge), Ge concentration (in pM), Ge/Si ratios (μmol/mol) and apparent oxygen utilization (AOU) at station WAP, Southern Ocean. Dashed lines indicate the limits between the water masses, AAIW, UCDW, LCDW and Antarctic Bottom Water (AABW).

Figure 6: Vertical profiles of Ge isotope composition ($\delta^{74/70}$Ge), Ge concentration (in pM), Ge/Si ratios (μmol/mol) and apparent oxygen utilization (AOU) at station Burdwood Bank, Southern Ocean. Dashed lines indicate the limits between the water masses, AAIW, UCDW, LCDW and AABW.

Figure 7: Relationship between dissolved Ge and Si concentrations at all three stations. The regression line (solid thin line) is calculated from the data reported in Table 1 and 2 and is defined by Ge = 0.775 ± 0.04 * Si + 3.6 ± 3.4, r^2 = 0.94. The thick dashed line corresponds to the regression line determined by Sutton et al. (2010) using a global seawater dataset and is defined by Ge = 0.760 ± 0.004 * Si + 1.27 ± 0.24, r^2 = 0.993).

Figure 8: Ge isotope composition of deep sea sponges against (a) Si isotope composition (data from Hendry et al., 2010) and (b) Ge/Si ratios. The relationships between Ge/Si ratios and Ge concentration in overlying seawater is also shown (c) and compared to previously reported correlation line from Ellwood et al. (2006) defined as Ge/Si = 0.0031 (± 0.0002) * Ge + 0.0818 (± 0.0078).

Figure 9: Salinity, temperature and oxygen profiles using CTD data from Robinson (2015). Thick black line represents CTD profile at WAP station, thick grey line represents CTD profile at Sars station and thin black line represents CTD profile at Burdwood Bank station. Markers correspond to discrete CTD values of seawater samples selected for Ge concentration and isotope composition (circles for WAP station, squares for SARS station and triangle for Burdwood Bank station). (a) Temperature-Salinity diagram of the three Southern Ocean stations studied covering the range of water depths sampled for Ge analysis. See text for the definition of water masses. (b) Vertical profiles of dissolved oxygen concentrations (mL/L) at the three stations. (c) Vertical profiles of salinity (psu) at the three stations.

Figure 10: $\delta^{74/70}$Ge vs Ge concentrations for the two stations (Sars, WAP) where surface seawater (< 1000m) was sampled. Water samples at depths greater than 1300m at station Sars are also shown for comparison. Solid line represents a Rayleigh fractionation model with initial $\delta^{74/70}$Ge = 2.4 ‰ and $\alpha_{liquid\text{-}solid}$ = 1.0006, the best fit for the upper 1000m water column

at station Sars. Dash line represents a Rayleigh fractionation model with initial $\delta^{74/70}Ge$ = 3.1 ‰ and $\alpha_{liquid\text{-}solid}$ = 1.0003, the best fit for the upper 1000m water column at station WAP and passing through the surface seawater of station Sars.

Table captions

Table 1: Germanium concentration and isotope composition of seawater samples from Loihi (N Pacific Ocean) and Bermuda (N Atlantic Ocean) areas

Table 2: Germanium concentration and isotope composition of seawater samples from the Southern Ocean recovered during cruise NBP1103. Ancillary parameters from CTD rosette are also reported

Table 3: Germanium concentration and isotope composition of deep sea sponges. Overlying seawater composition is also reported.

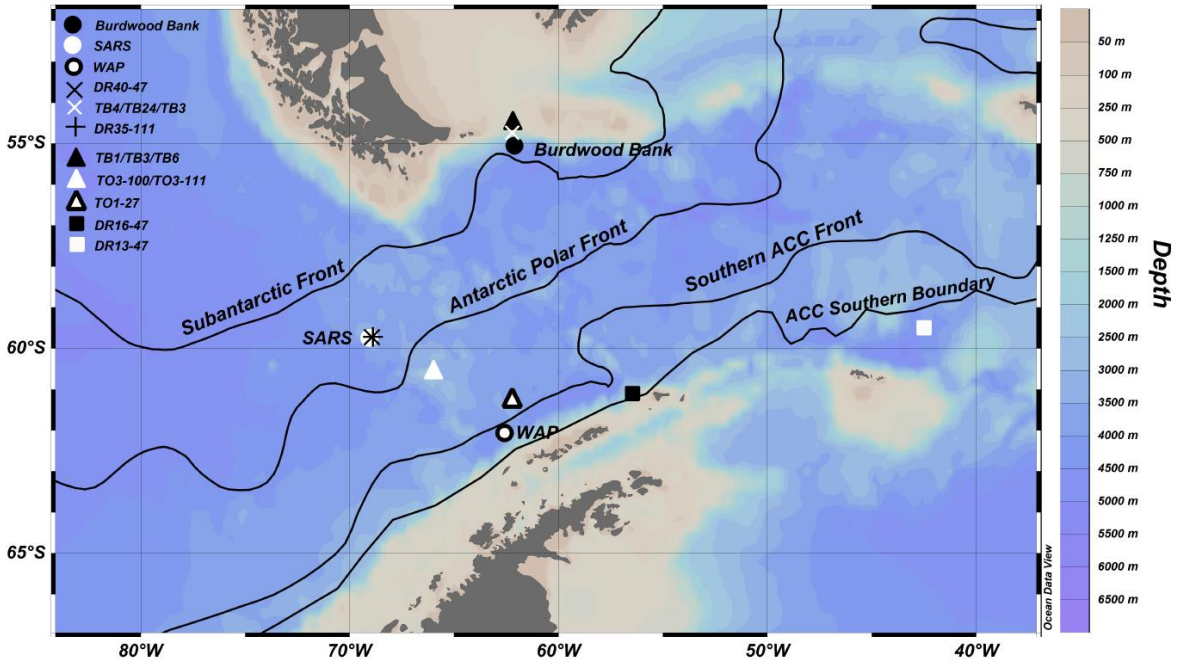
Burdwood Bank
SARS
WAP
DR40-47
TB4/TB24/TB3
DR35-111
TB1/TB3/TB6
TO3-100/TO3-111
TO1-27
DR16-47
DR13-47
Subantarctic Front
Antarctic Polar Front
Southern ACC Front
ACC Southern Boundary
55°S
60°S
65°S
80°W
70°W
60°W
50°W
40°W
Depth
50 m
100 m
250 m
500 m
750 m
1000 m
1250 m
1500 m
2000 m
2500 m
3000 m
3500 m
4000 m
4500 m
5000 m
5500 m
6000 m
6500 m
Ocean Data View

1050

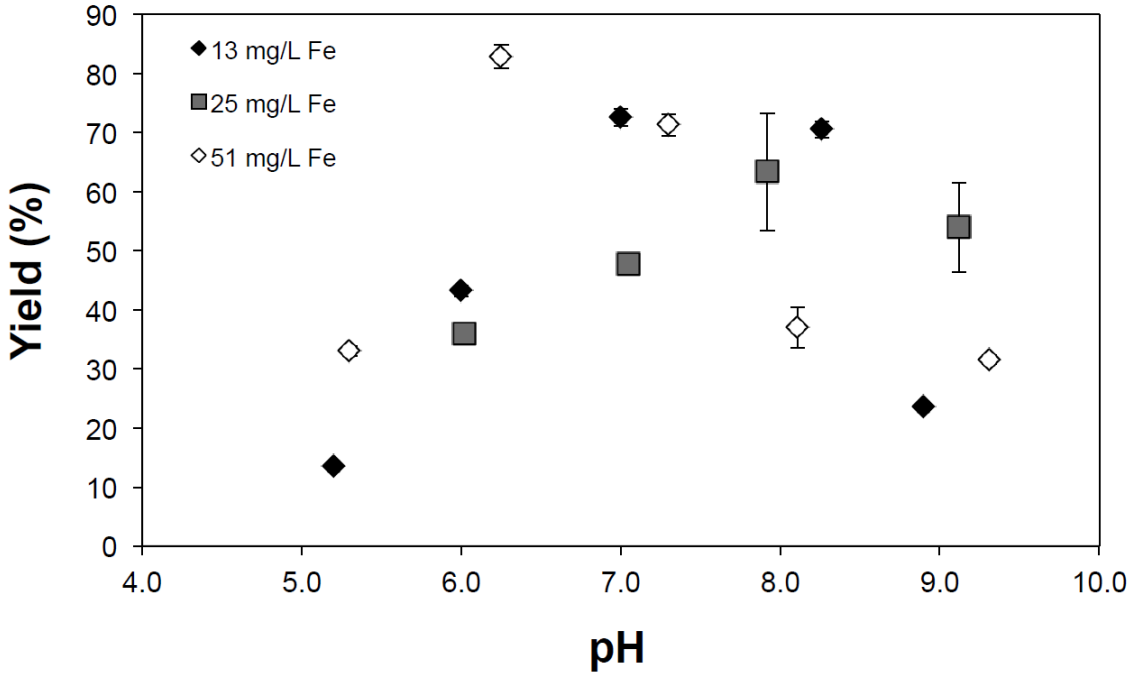
13 mg/L Fe
25 mg/L Fe
51 mg/L Fe
Yield (%)
pH
0
10
20
30
40
50
60
70
80
90
4.0
5.0
6.0
7.0
8.0
9.0
10.0

1051

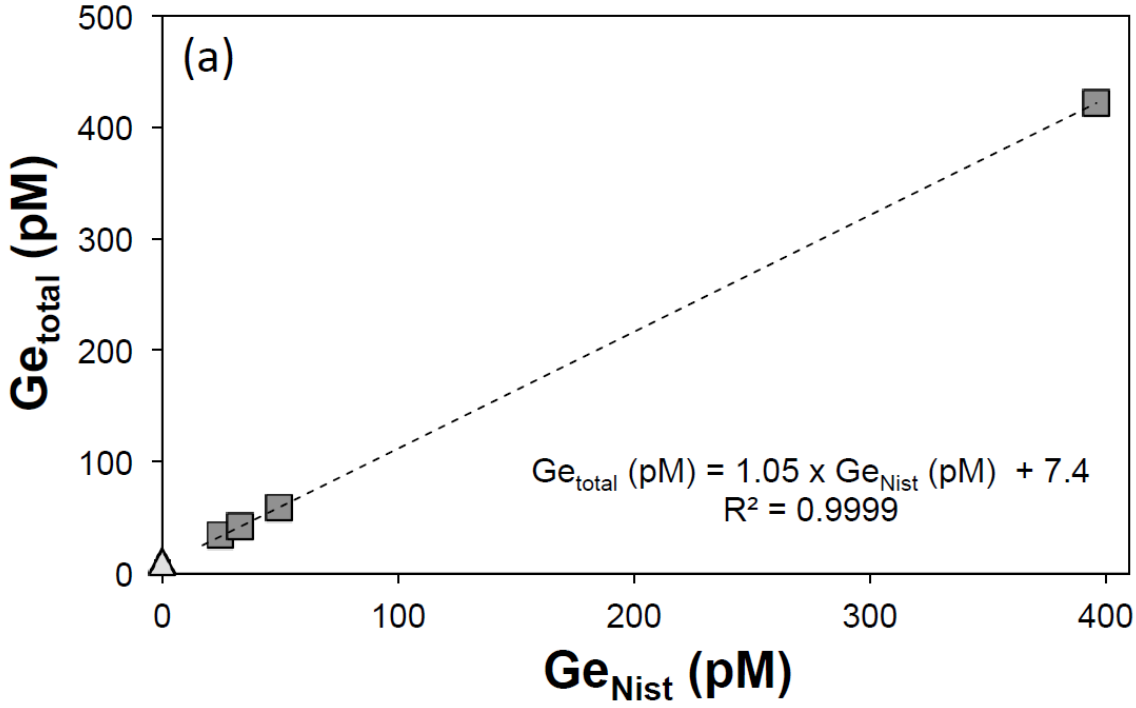
(a)
Ge_total (pM) = 1.05 x Ge_Nist (pM) + 7.4
R² = 0.9999
Ge_total (pM)
Ge_Nist (pM)
0
100
200
300
400
500

1052

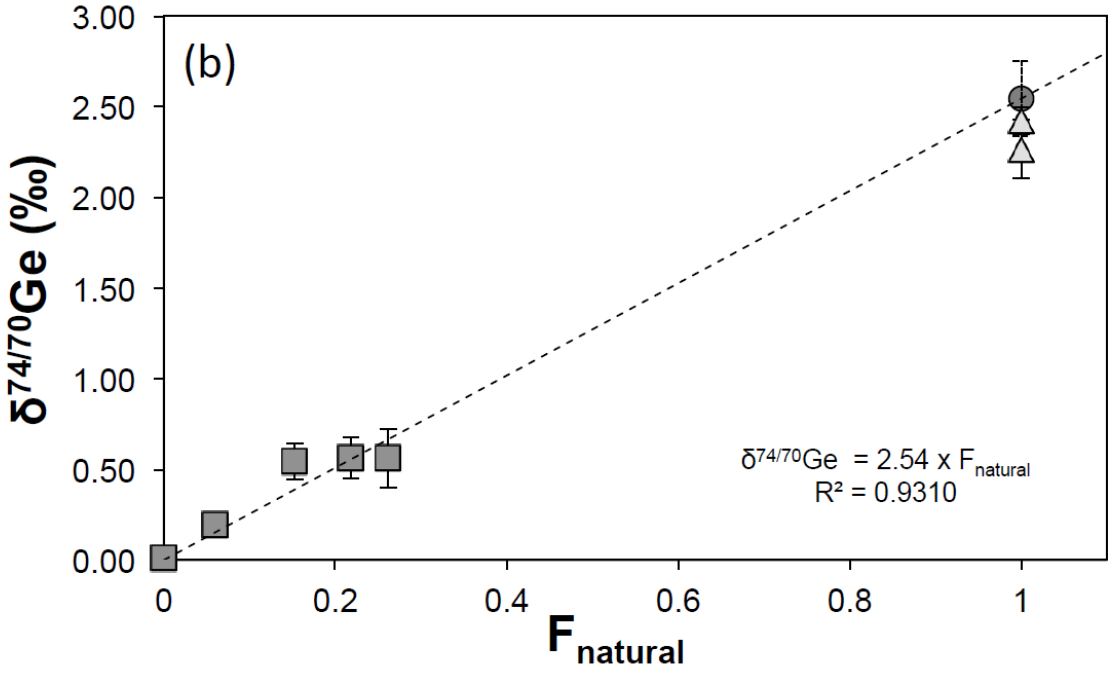
(b)
δ74/70Ge = 2.54 x F_natural
R² = 0.9310
δ74/70Ge (‰)
F_natural
0.00
0.50
1.00
1.50
2.00
2.50
3.00
0
0.2
0.4
0.6
0.8
1

1053

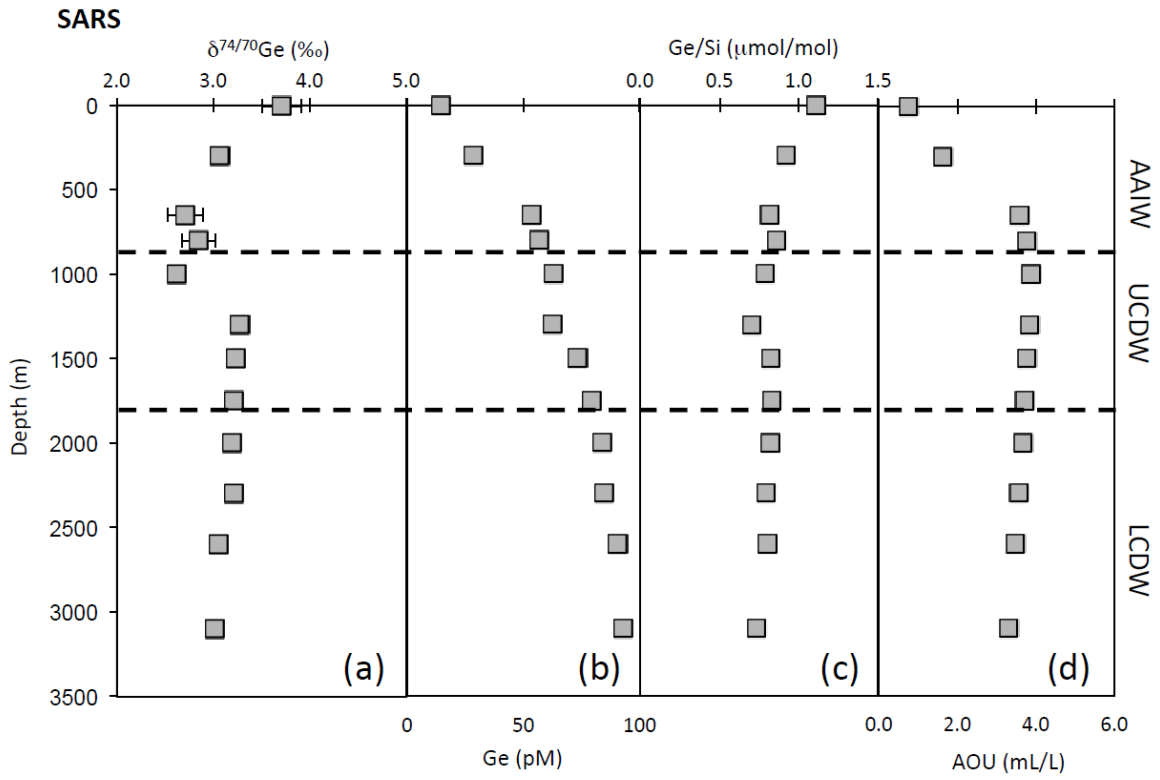
SARS
δ74/70Ge (‰)
Ge/Si (μmol/mol)
Depth (m)
Ge (pM)
AOU (mL/L)
AAIW
UCDW
LCDW
(a)
(b)
(c)
(d)

1054

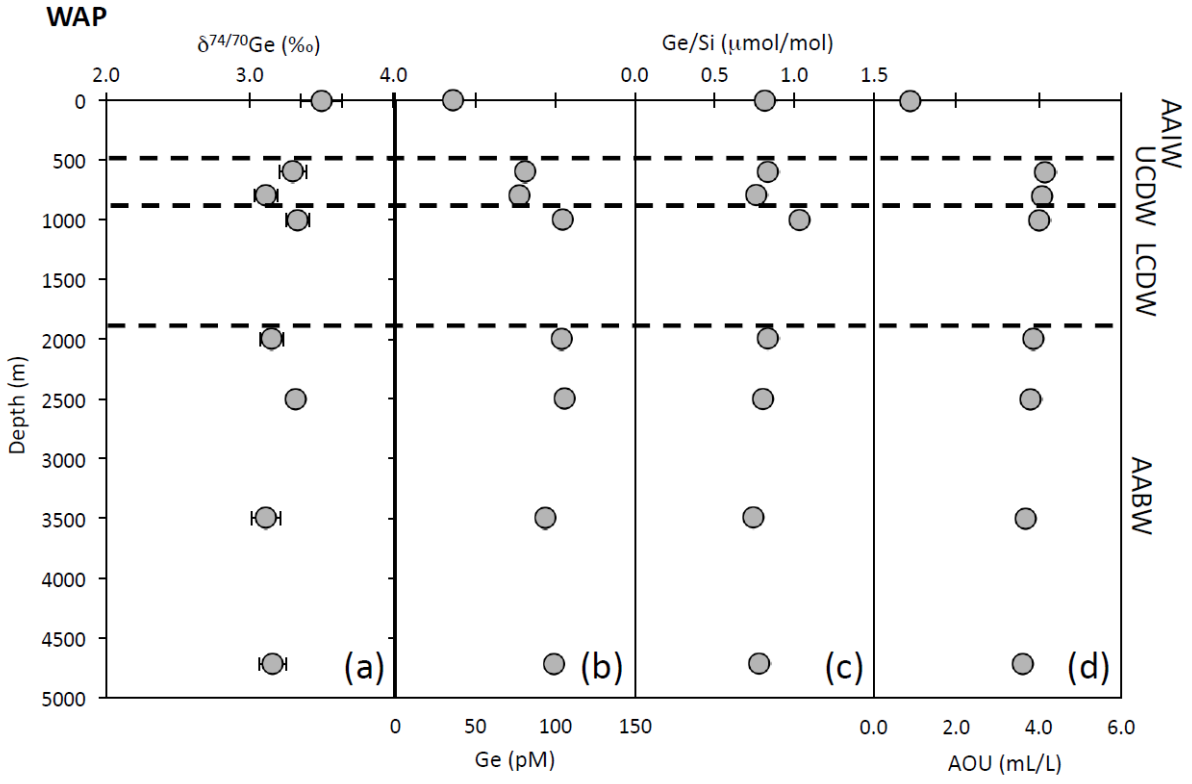
WAP
δ74/70Ge (‰)
Ge/Si (μmol/mol)
Depth (m)
Ge (pM)
AOU (mL/L)
AAIW
UCDW
LCDW
AABW
(a)
(b)
(c)
(d)

1055

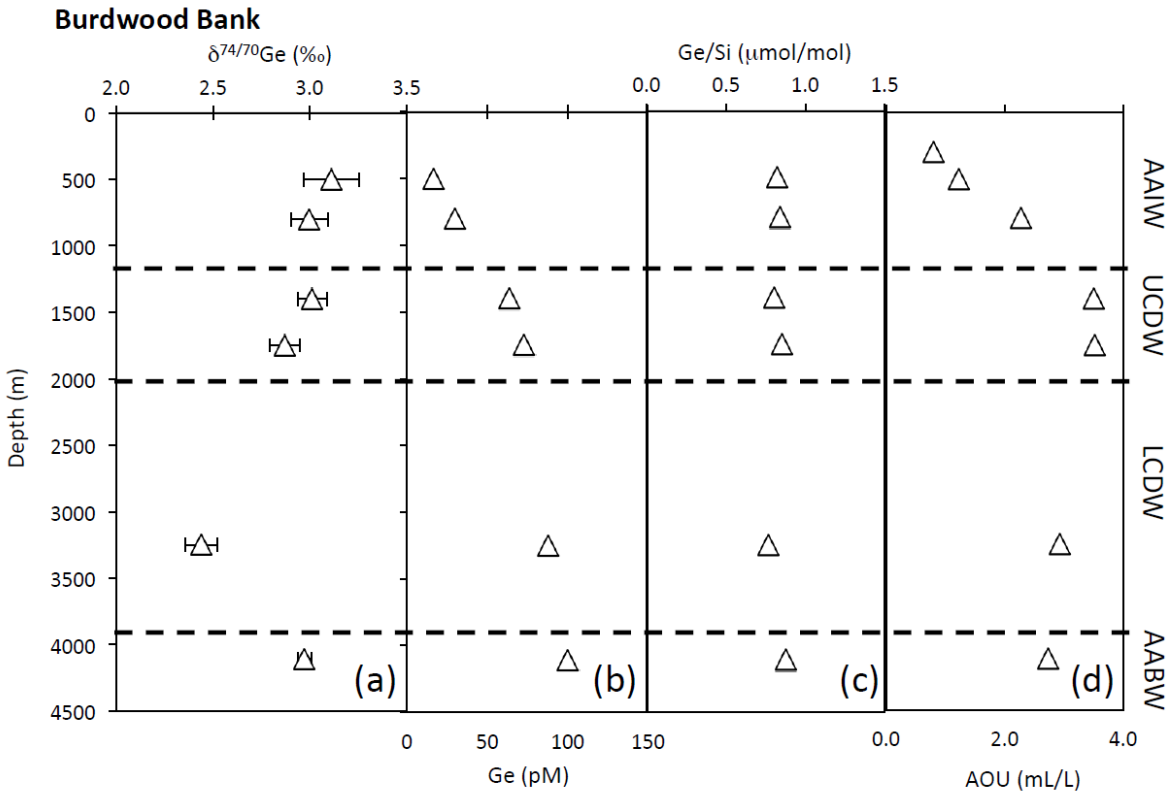
Burdwood Bank
δ74/70Ge (‰)
Ge/Si (μmol/mol)
Depth (m)
Ge (pM)
AOU (mL/L)
AAIW
UCDW
LCDW
AABW
(a)
(b)
(c)
(d)

1056

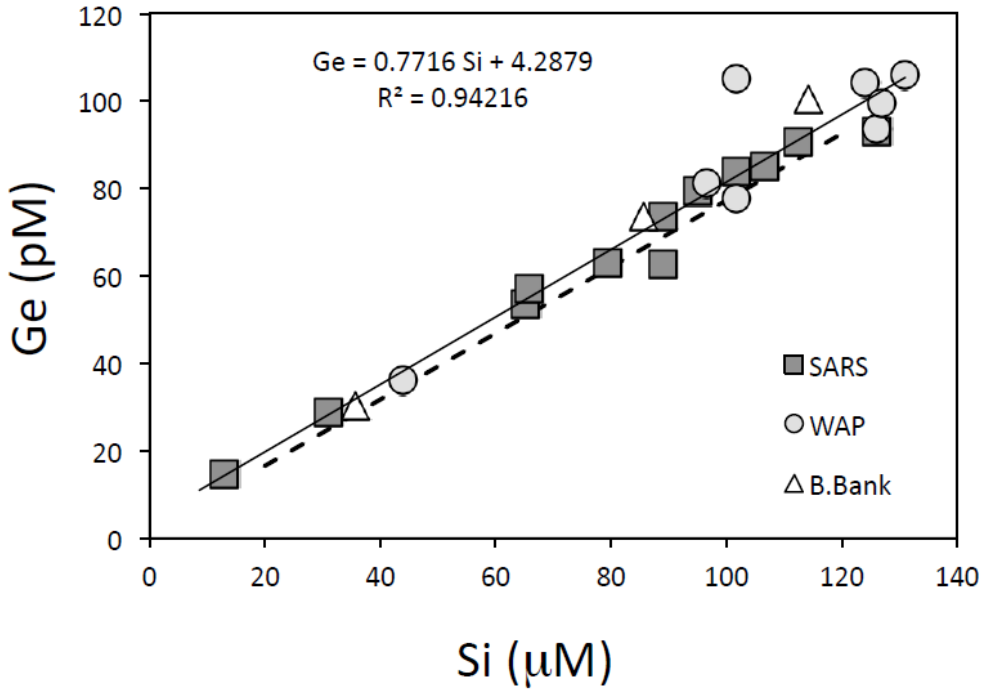
Ge = 0.7716 Si + 4.2879
R² = 0.94216
SARS
WAP
B.Bank
Ge (pM)
Si (μM)

1057

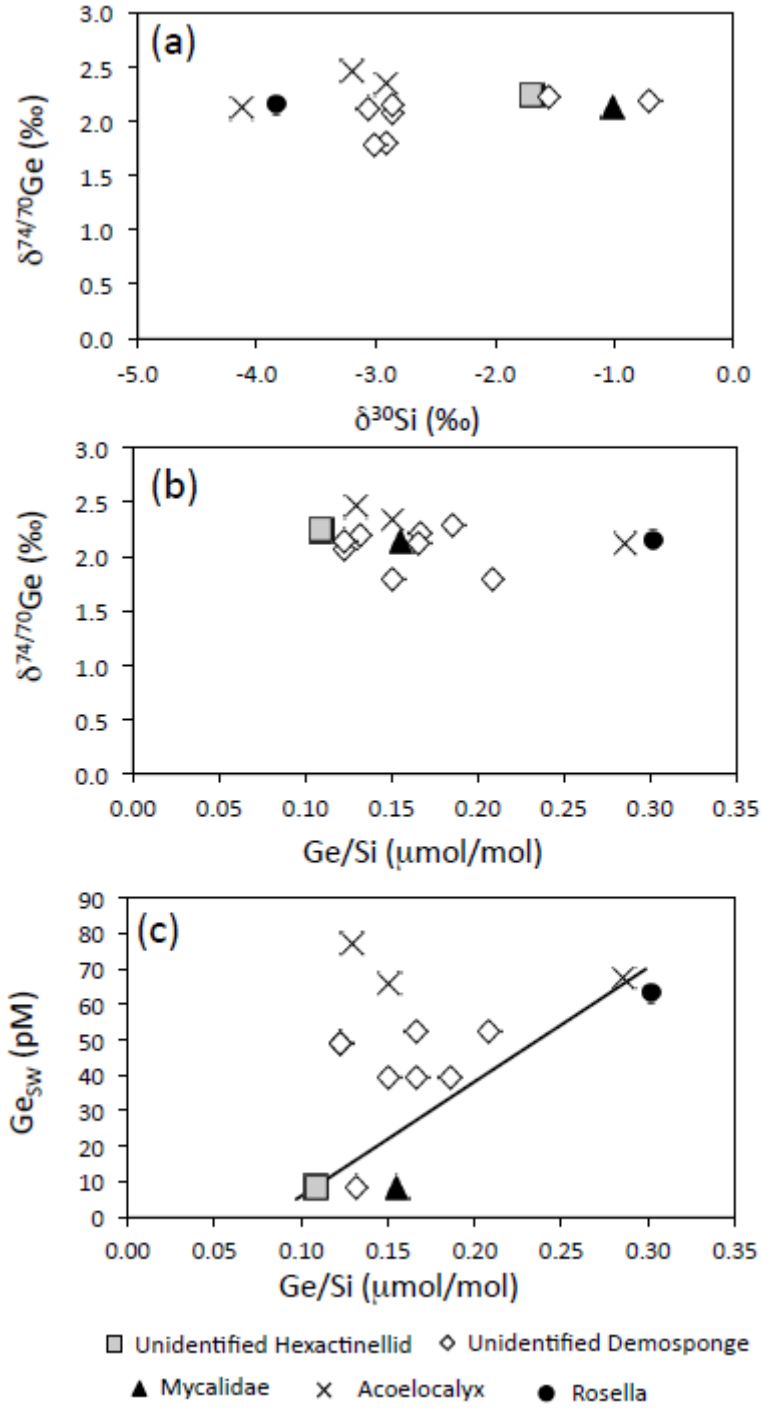
(a)
δ74/70Ge (‰)
δ30Si (‰)
(b)
δ74/70Ge (‰)
Ge/Si (µmol/mol)
(c)
GeSW (pM)
Ge/Si (µmol/mol)
Unidentified Hexactinellid
Unidentified Demosponge
Mycalidae
Acoelocalyx
Rosella

1058

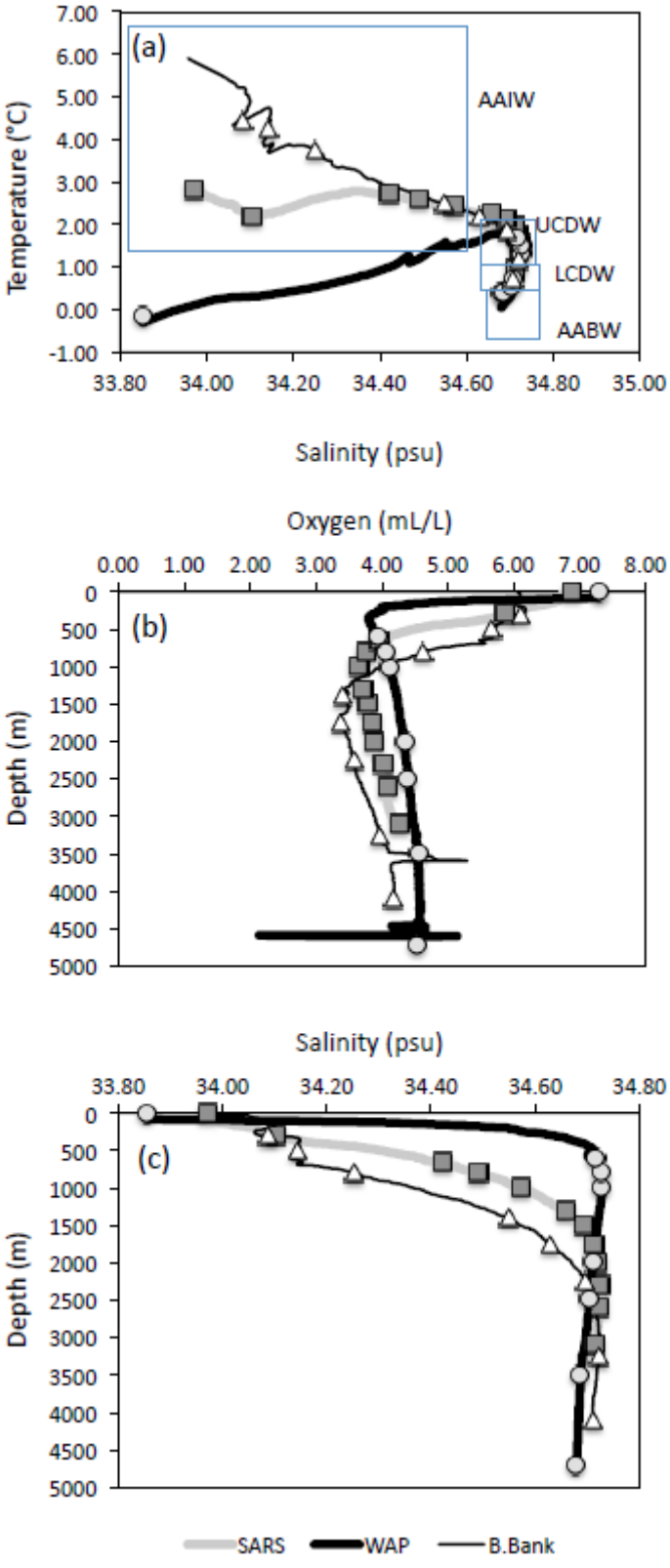
(a)
AAIW
UCDW
LCDW
AABW
Temperature (°C)
Salinity (psu)
(b)
Oxygen (mL/L)
Depth (m)
(c)
Salinity (psu)
Depth (m)
SARS
WAP
B.Bank

1059

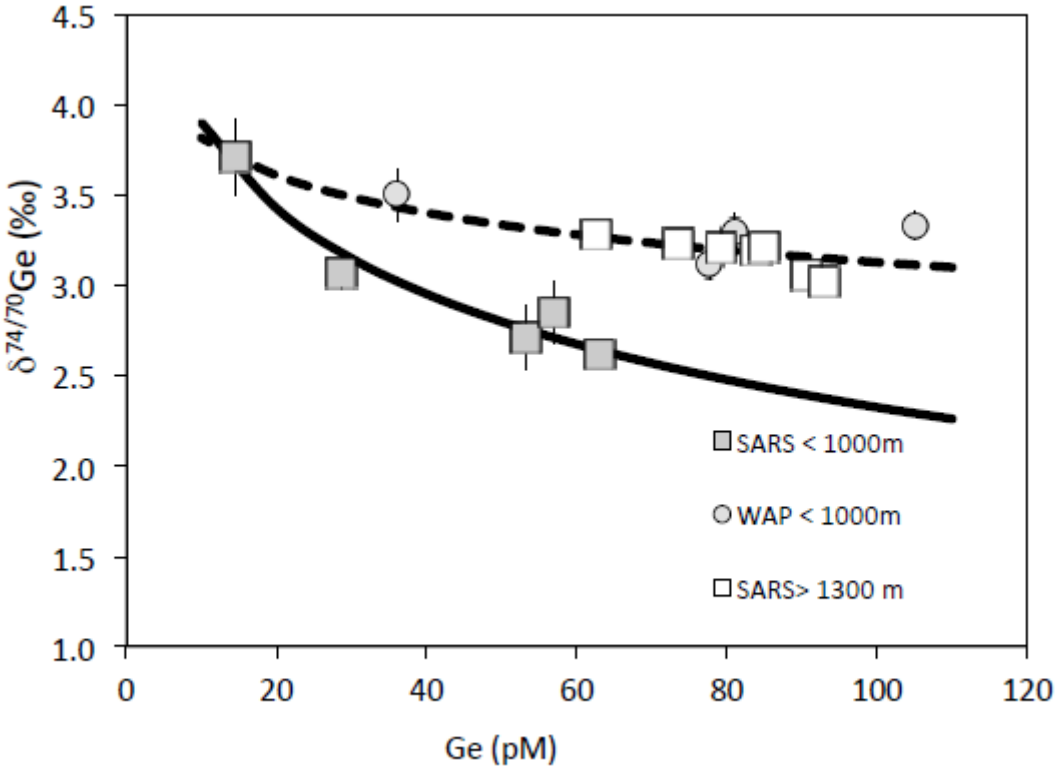
4.5
4.0
3.5
3.0
2.5
2.0
1.5
1.0
δ74/70Ge (‰)
0
20
40
60
80
100
120
Ge (pM)
SARS < 1000m
WAP < 1000m
SARS> 1300 m

1060